

國立交通大學

電子工程學系電子研究所

博 士 論 文

在快速時變且多重路徑通道下使用白化處理於殘留載波
間干擾和通道雜訊的正交分頻多工訊號接收

OFDM Signal Detection in Doubly Selective Channels with
Whitening of Residual Inter-carrier Interference and Noise



研 究 生：王海薇

指 導 教 授：林大衛博士
桑梓賢博士

中 華 民 國 一 百 零 一 年 七 月

在快速時變且多重路徑通道下使用白化處理於殘留載波間干擾和通
道雜訊的正交分頻多工訊號接收

OFDM Signal Detection in Doubly Selective Channels with
Whitening of Residual Intercarrier Interference and Noise

研 究 生：王海薇

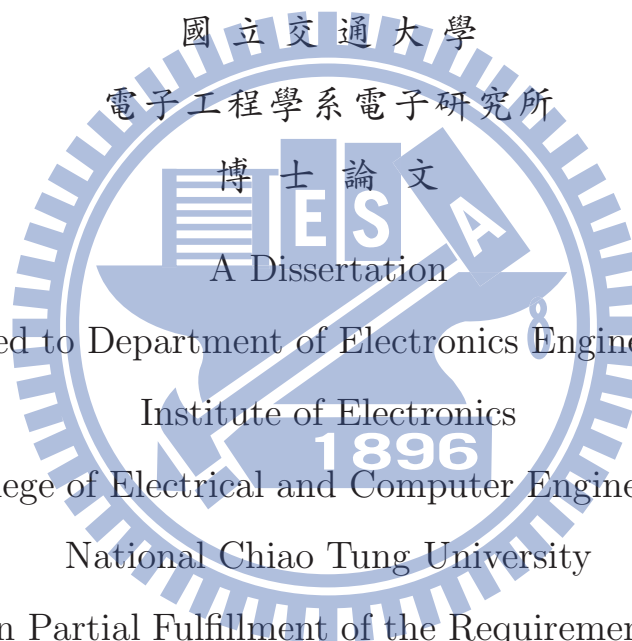
Student: Hai-wei Wang

指 導 教 授：林大衛博士

Advisors: Dr. David W. Lin

桑梓賢博士

Dr. Tzu-Hsien Sang



Submitted to Department of Electronics Engineering and
Institute of Electronics
College of Electrical and Computer Engineering
National Chiao Tung University
in Partial Fulfillment of the Requirements

for the Degree of
Doctor of Philosophy

in

Electronics Engineering

July 2012

Hsinchu, Taiwan, Republic of China

中華民國一百零一年七月

在快速時變且多重路徑通道下使用白化處理於殘留載波間干擾和通道雜訊的正交分頻多工訊號接收

學生：王海薇

指導教授：林大衛博士
桑梓賢博士

國立交通大學電子工程學系電子研究所

摘要

在正交分頻多工(OFDM)通訊系統下，載波頻率飄移或通道時變導致載波間干擾(ICI)和傳輸效能的衰減。當載波頻率非常高或用戶端移動速度很快時，這個問題特別嚴重。載波間干擾讓通道矩陣不再只有對角方向有值，這種情形使得正交分頻多工信號接收變得很困難。理論上，一個最佳的訊號偵測器應該考慮所有的載波間干擾項。但是考慮複雜度和穩健前提下，習知的方法通常只有針對集中於對角項附近的主要項補償，而且將未被補償的殘留載波(residual ICI)間干擾視為通道白色雜訊的一部分。

本論文利用能帶近似法(band approximation)將含有載波間干擾(ICI)的訊號劃分成三個部份，其中包含一主要訊號、一殘留的載波間干擾(residual ICI)以及一通道雜訊。透過公式逼近、理論推導和通道模擬的方法讓我們觀察到相鄰次載波之殘留的載波間干擾(residual ICI)具有高度的正規化相關性之統計特性，並且特別的是，我們可根據該統計特性將因考量接收器的複雜度而不得而被捨棄之殘留的載波間干擾(residual ICI)項全部考慮進去。甚至，我們發現該相鄰次載波之殘留的載波間干擾(residual ICI)的正規化相關性在幾乎所有實際應用的系統參數下是不變的，該系統參數包含最大多普勒頻率位移(maximum Doppler shift)、多重路徑通道數據(multipath channel profile)、功率頻譜密度(power spectral density)、正交分頻多工系統之取樣週期(sampling period)、離散傅利葉轉換之長度(DFT size)、正交性分頻多工系統之符號週期(symbol period)以及平均傳送符號能(average transmitted symbol energy)。以上的發現說明了該相鄰次載波之殘留的載波間干擾(residual ICI)高度的正規化相關性和容易估計的特性非常適合應用於實際通訊系統接收。

利用該統計特性，透過針對殘留的載波間干擾(residual ICI)和通道雜訊進行

白化處理的一接受器可以得到非常低的雜訊底(noise floor)，進而使通訊系統具有很好的傳輸性能，例如電腦模擬顯示採用最大可能序列估計(maximum-likelihood sequence estimation, MLSE)的接收器 並且考慮上述白化處理用於該相鄰載波之殘留的載波間干擾(residual ICI)可以降低位元誤差率(BER)之誤差底(error floor) 數個級數(order)，可明顯看出利用該統計特性結合傳統接收偵測方法對於提升通訊系統之接收效能有很大的貢獻。

更進一步，本論文提供一個考慮上述白化程序用於“相鄰載波所殘留的載波間干擾”的線性最小均方誤差(LMMSE)和遞迴線性最小均方誤差接收器。相對於最大可能序列估計，這個方法在良好的偵測性能和低複雜度間提供另一折衷選擇。



OFDM Signal Detection in Doubly Selective Channels with Whitening of Residual Intercarrier Interference and Noise

Student: Hai-wei Wang

Advisors: Dr. David W. Lin
Dr. Tzu-Hsien Sang

Department of Electronics Engineering
& Institute of Electronics
National Chiao Tung University

ABSTRACT

Orthogonal frequency-division multiplexing (OFDM) is a popular broadband wireless transmission technique, but its performance can suffer severely from the inter-carrier interference (ICI) induced by fast channel variation arising from high-speed motion. Existing ICI countermeasures usually address a few dominant ICI terms only and treat the residual similar to white noise.

We show that the residual ICI has high normalized autocorrelation and that this normalized autocorrelation is insensitive to the maximum Doppler frequency and the multipath channel profile, the OFDM sample period, the discrete Fourier transform (DFT) size, the OFDM symbol time, the transmitted symbol energy. Consequently, the residual ICI plus noise can be whitened in a nearly channel-independent manner, leading to significantly improved detection performance. Simulation results confirm the theoretical analysis. As a result, a whitening transform for the residual ICI plus noise can be obtained based solely on the ICI-to-noise ratio. Such a transform can be used in association with many different signal detection schemes to significantly improve the detection performance.

In particular, they show that the proposed technique can significantly lower the ICI-induced error floor by several orders of magnitude in maximum-likelihood sequence estimation (MLSE) designed to address a few dominant ICI terms. For QPSK, the proposed method can lower the error floor induced by ICI to under 10^{-6} with MLSE that takes into account two nearest-neighbor ICI terms with perfect

channel state information (CSI).

Furthermore, we consider linear minimum mean-square error (LMMSE) and iterative LMMSE detection with the above partial whitening of additive disturbance, together with soft decision feedback. The method is shown to provide good performance-complexity tradeoff compared to other ICI countermeasures.

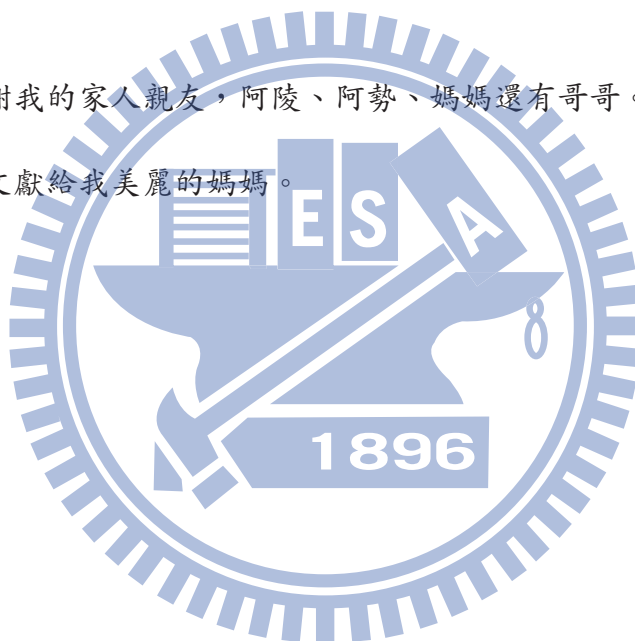


誌 謝

首先，我要感謝林大衛老師和桑梓賢老師的指導。還有星期二博士班討論會議上的伙伴，欣德、俊榮和 Albert。感謝大家熱心地與我討論，真的給我很大的幫助。

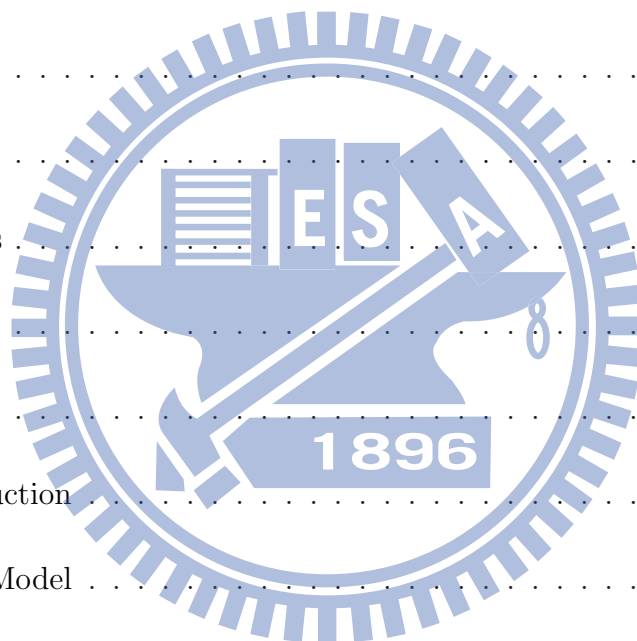
其次，我感謝我的家人親友，阿陵、阿勢、媽媽還有哥哥。

最後，這論文獻給我美麗的媽媽。



Contents

書名頁	i
中文摘要	ii
Abstract	iv
誌謝	vi
Table of Contents	vii
List of Tables	x
List of Figures	xi
1 Thesis Introduction	1
1.1 System Model	4
1.2 Thesis Organization and Contributions	5
2 Wireless Channel Characterization	8
2.1 Wireless Channel	8
2.2 Multipath Fading	9
2.2.1 Statistical Characterization of Multipath Channels	10
2.2.2 Doubly Selective Channel Model	10
2.3 Statistical Characterization of the Time-Variant Behavior	11



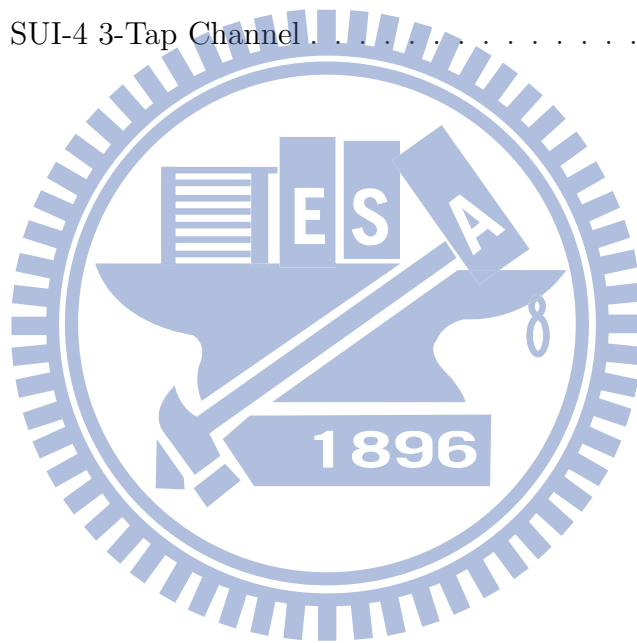
2.4	Statistical Characterization: The WSSUS Model	12
2.5	The Time-Varying Channel	13
2.5.1	Jakes Doppler Spectrum	13
2.5.2	Doppler Spreading Simulation	14
3	Autocorrelation of Residual Intercarrier Interference	16
3.1	Derivation of Autocorrelation of Residual ICI	17
3.2	Numerical Examples	21
3.3	Derivation of (3.6) and Some Related Comments	30
3.4	Summary of Results	32
4	MLSE Detection with Whitening of Residual ICI Plus Noise	33
4.1	MLSE Detection with Whitening of Residual ICI Plus Noise	34
4.2	Complexity Analysis	37
4.3	Simulation Results on Detection Performance	38
4.4	Dependence of Detection Performance on Parameter Setting	45
4.5	Summary of Results	48
5	Low Complexity Detection with Whitening of Residual ICI Plus Noise	49
5.1	LMMSE Signal Detection with Whitening of Residual ICI Plus Noise	50
5.2	Simulation Results	53
5.3	Summary of Results	57
6	Thesis Conclusions and Potential Future Topics	58
6.1	Thesis Conclusions	58
6.2	Potential Future Research Topics	60

Appendix A: The Whiteners of Residual ICI Plus Noise	61
簡歷	72
著作目錄	73



List of Tables

4.1 Two Channel Power-Delay Profiles Used in This Study, Where TU6
Corresponds to the COST 207 6-Tap Typical Urban Channel And
SUI4 the SUI-4 3-Tap Channel 37



List of Figures

1.1	OFDM system model.	2
2.1	Frequency Selective Fading Channel Simulators.	11
3.1	Normalized autocorrelation of residual ICI over multipath Rayleigh fading channel at $K = 0$, with $N = 128$ and $T_{sa} = 714$ ns. The first-order approximation (3.11)–(3.13) yields 0.6079 for $r = 1$ and 0.1520 for $r = 2$, which are quite accurate at low f_d values.	22
3.2	Normalized autocorrelation of residual ICI over multipath Rayleigh fading channel at $K = 1$, with $N = 128$ and $T_{sa} = 714$ ns. The first-order approximation (3.11)–(3.13) yields 0.7753, 0.6461, 0.5599, 0.3036, 0.1912, and 0.1317, for $r = 1$ –6, respectively, which are quite accurate.	23
3.3	Normalized autocorrelation of residual ICI over multipath Rayleigh fading channel at $K = 2$, with $N = 128$ and $T_{sa} = 714$ ns. The first-order approximation (3.11)–(3.13) yields 0.8440, 0.7358, 0.6612, 0.6014, and 0.5534, for $r = 1$ –5, respectively, which are quite accurate.	24
3.4	Normalized autocorrelation of residual ICI over one-Doppler-line channel at $K = 0$, with $N = 128$ and $T_{sa} = 714$ ns.	25
3.5	Normalized autocorrelation of residual ICI over one-Doppler-line channel at $K = 1$, with $N = 128$ and $T_{sa} = 714$ ns.	26

3.6	Normalized autocorrelation of residual ICI over one-Doppler-line channel at $K = 2$, with $N = 128$ and $T_{sa} = 714$ ns.	27
4.1	Trellis structure for MLSE-based detection using the Viterbi algorithm, under QPSK modulation and with $p = 1$, where numerals 0–3 represent the QPSK constellation points.	36
4.2	Error performance in TU6 channel of the conventional OFDM signal detection method and ICI-whitening MLSE (the proposed method) with $K = 0$ and $p = q = 1$ in noise-free condition.	41
4.3	Comparison of proposed technique in TU6 and SUI4 channels with that treating residual ICI as white; $\text{SNR} = \infty$	42
4.4	Performance of proposed technique versus Doppler spread in the TU6 channel with $p = q = K = 1$, at $N = 128$ and $T_{sa} = 714$ ns and under QPSK subcarrier modulation.	43
4.5	Performance versus E_b/N_0 of different methods in the TU6 channel, with $N = 128$, $T_{sa} = 714$ ns, $f_d = 1500$ Hz (normalized peak Doppler frequency $f_d T_{sa} N = 0.1371$) and QPSK subcarrier modulation. (Results with $N = 1024$ are very close.)	44
4.6	SINR performance of different methods in the TU6 channel, with $N = 128$ and $T_{sa} = 714$ ns and assuming perfect CSI.	47
5.1	Bit error rate of different detection methods in the TU6 channel, with $N = 128$, $T_{sa} = 714$ ns, $f_d = 1500$ Hz (normalized peak Doppler frequency $f_d T_{sa} N = 0.1371$) and QPSK subcarrier modulation.	54
5.2	Bit error rate floor versus Doppler spread of different detection methods in the TU6 channel with $N = 128$, $T_{sa} = 714$ ns, and QPSK subcarrier modulation.	55

5.3	Bit error rate floor versus Doppler spread of different detection methods in the TU6 channel with $N = 128$, $T_{sa} = 714$ ns, and 16QAM subcarrier modulation.	56
A.1	Performance of proposed MLSE $p = q = K = 1$ and MMSE $p = q = 1, K = 2$, with imperfect whitener in the TU6 channel, at $N = 128$ and $T_{sa} = 714$ ns $f_d T_{sa} N = 0.137$ and under QPSK subcarrier modulation.	66



Chapter 1

Thesis Introduction

Orthogonal frequency-division multiplexing (OFDM) is widely adopted in broadband wireless signal transmission due to its high spectral efficiency. However, its performance can suffer severely from the intercarrier interference (ICI) induced by fast channel variation resulting from high-speed motion. Such an effect is sometimes referred to as loss of subcarriers orthogonality. The problem becomes increasingly acute as the carrier frequency or the speed of motion increases. For instance, with a 500 km/h mobile speed and a 6 GHz carrier frequency, the peak Doppler frequency can be as high as about 2800 Hz, which translates to over 0.25 times the 10.94 kHz subcarrier spacing in the Mobile WiMAX standard [1]. The signal detection performance can become intolerable without proper countermeasures.

Consider the typical OFDM system illustrated in Fig. 1.1. In a system without ICI, the channel frequency response matrix that relates the inputs of the inverse discrete Fourier transform (IDFT) and the outputs of the DFT is diagonal. Fast channel variation introduces sizable off-diagonal elements in the matrix, thus resulting in ICI.

The direct minimum mean square error and zero-forcing equalizers for OFDM symbols requires a large matrix inversion. Several algorithms [14–16] were developed to reduce the complexity of this direct matrix inverse for OFDM symbols .

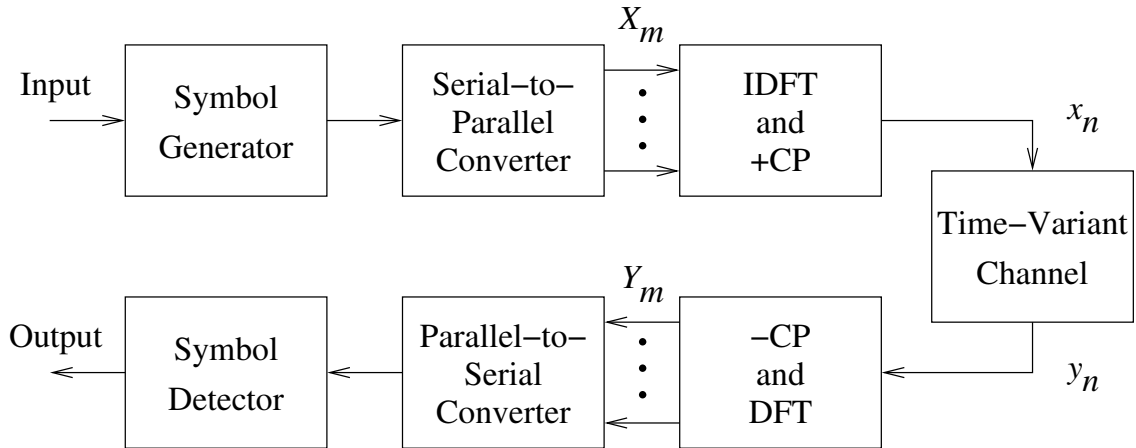


Figure 1.1: OFDM system model.

Choi et al. [14] proposed a MMSE equalizer for OFDM symbols incorporating with successive interference cancellation. In [15], Cai and Giannakis derived recursive algorithms for calculation of the matrix inversion by combining the methods [2,15].

The above equalizers [14,15] still require $\geq O(N^2)$ complexity, where N is the number of subcarriers. Hsu and Wu [16] proposed a successive detection combined with Newton's iterative matrix inversion, requiring $O(N \log N)$ complexity. However, as the subcarrier numbers in one OFDM symbol increases, the direct implementation of a traditional MMSE or ZF equalizer should be avoided.

In theory, an optimal signal detector should take all ICI terms into account. But for reasons of complexity and robustness, usually only the dominant terms are compensated for. As these dominant terms are normally concentrated (circulantly) around the diagonal, the channel matrix shows a (circulant) band structure [2–4,22].

Several frequency-domain equalization techniques based on band approximation to channel matrices have been proposed, including blockwise zero-forcing linear equalization [2], linear minimum mean-square error (LMMSE) equalization [3,22,23], and maximum-likelihood sequence estimation (MLSE) [4].

An interested reader may refer to [16] for additional introduction to various ICI mitigation studies.

Jeon *et al.* [2] consider the situation where the normalized peak Doppler frequency (i.e., peak Doppler frequency expressed in units of frequency spacing of subcarriers) is on the order of 0.1 or less. In this situation, the channel variation over one OFDM symbol time is approximately linear. A frequency-domain equalizer that exploits the ensuing band channel matrix structure is proposed. Schniter [22] considers substantially higher normalized peak Doppler frequencies, under which the ICI is more widespread. Time-domain windowing is used to partially counteract the effect of channel variation and shrink the bandwidth of the channel matrix. An iterative minimum mean-square error (MMSE) equalizer is then used to detect the signal. Rugini *et al.* [3] employ block-type linear MMSE equalization, wherein the band channel matrix structure is exploited (via triangular factorization of the autocorrelation matrix) to reduce the equalizer complexity. Ohno [4] addresses the ICI via maximum-likelihood sequence estimation (MLSE) in the frequency domain, where the band channel matrix structure is utilized to limit the trellis size.

The consideration of only the dominant ICI terms results in an irreducible error floor in time-varying channels [2–4,22]. Moreover, while the uncompensated residual ICI is colored [5,6,24], for various reasons it is often treated as white [4–7,24].

In principle, the error performance floor can be reduced by whitening. Although whitening of “I+N” (i.e., sum of ICI and additive channel noise) can lead to improved signal detection performance, it requires knowing the autocorrelation function of I+N, which remains a key problem awaiting solution [6,24]. Without knowing the autocorrelation function, one can only resort to less sophisticated techniques, such as simple differencing of the received signals at neighboring subcarriers [8]. Authors [8] further point out that the noise and channel statistics is a challenging and interesting problem under investigation.

In this thesis, we attempt to characterize this autocorrelation function of residual ICI plus noise for the benefit of signal detection.

1.1 System Model

Fig. 1.1 shows the discrete-time baseband equivalent model of the considered OFDM system. The input-output relation of the channel is given by

$$y_n = \sum_{l=0}^{L-1} h_{n,l} x_{n-l} + w_n \quad (1.1)$$

where x_n and y_n are, respectively, the channel input and output at time n , L is the number of multipaths, $h_{n,l}$ is the complex gain of the l th path (or tap) at time n , and w_n is the complex additive white Gaussian noise (AWGN) at time n . We assume that the length of the cyclic prefix (CP) is sufficient to cover the length of the channel impulse response (CIR) $(L-1)T_{sa}$, where T_{sa} denotes the sampling period.

One common way of expressing the received signal in the DFT domain is

$$Y_m = \sum_{k=0}^{N-1} \sum_{l=0}^{L-1} X_k H_l^{(m-k)} e^{-j2\pi lk/N} + W_m, \quad 0 \leq m \leq N-1, \quad (1.2)$$

where X_k and Y_m are, respectively, the channel input and output in the frequency domain (see Fig. 1.1), N denotes the size of DFT, W_m denotes the DFT of w_m , and $H_l^{(k)}$ is the frequency spreading function of the l th path given by

$$H_l^{(k)} = \frac{1}{N} \sum_{n=0}^{N-1} h_{n,l} e^{-j2\pi nk/N}. \quad (1.3)$$

Another way of expressing it is

$$\mathbf{y} = \mathbf{H}\mathbf{x} + \mathbf{w} \quad (1.4)$$

where $\mathbf{y} = [Y_0, \dots, Y_{N-1}]'$, $\mathbf{x} = [X_0, \dots, X_{N-1}]'$, $\mathbf{w} = [W_0, \dots, W_{N-1}]'$, and

$$\mathbf{H} = \begin{bmatrix} a_{0,0} & a_{0,1} & \cdots & a_{0,N-1} \\ a_{1,0} & a_{1,1} & \cdots & a_{1,N-1} \\ \vdots & \vdots & \ddots & \vdots \\ a_{N-1,0} & a_{N-1,1} & \cdots & a_{N-1,N-1} \end{bmatrix}, \quad (1.5)$$

with $'$ denoting transpose and

$$a_{m,k} = \sum_{l=0}^{L-1} H_l^{(m-k)} e^{-j2\pi kl/N}. \quad (1.6)$$

The quantity $a_{m,k}$ is the ‘‘ICI coefficient’’ from subcarrier k to subcarrier m . For a time-invariant channel, $H_l^{(k)}$ vanishes $\forall k \neq 0$ and \mathbf{H} becomes diagonal, implying absence of ICI.

As mentioned, a band approximation to \mathbf{H} that retains only the dominant terms about the diagonal may ease receiver design and operation, but also results in an irreducible error floor. Consider a symmetric approximation with one-side bandwidth K , that is, $a_{m,k} = 0$ for $|(m - k)\%N| > K$ where K is a nonnegative integer and $\%$ denotes modulo operation. Then the ICI at each subcarrier consists of contributions from at most $2K$ nearest (circularly) subcarriers. In this chapter, we exploit the correlation of the residual ICI *outside* the band to attain a significantly enhanced signal detection performance. For convenience, in the following we omit explicit indication of modulo- N in indexing a length- N sequence, understanding an index, say n , to mean $n\%N$.

Let the channel be wide-sense stationary uncorrelated scattering (WSSUS) [10] with

$$E[h_{n,l}h_{n-q,l-m}^*] = \sigma_l^2 r_l(q)\delta(m) \quad (1.7)$$

where $E[\cdot]$ denotes expectation, σ_l^2 denotes the variance of the l th tap gain, $r_l(q)$ denotes the normalized tap autocorrelation (where $r_l(0) = 1$), and $\delta(m)$ is the Kronecker delta function. For convenience, assume $\sum_l \sigma_l^2 = 1$. Let $P_l(f)$ denote the Doppler power spectral density (PSD) of path l and thus

$$r_l(q) = \left[\int_{-f_d}^{f_d} P_l(f) e^{j2\pi f\tau} df \right] \Big|_{\tau=T_{sa}q}, \quad (1.8)$$

where f_d denotes the peak Doppler frequency of the channel. We assume that the paths may be subject to arbitrary, different fading so that $P_l(f)$ may be asymmetric about $f = 0$ and different for different l .

1.2 Thesis Organization and Contributions

The content of Chap. 3,4 has been published in [9,25] and the content of Chap. 5 will be published in [40].

The contribution of the present thesis is twofold.

First, we explore the correlation property of ICI outside the band and derive an approximate mathematical expression for it. The expression applies not only to classical multipath Rayleigh fading, but also to arbitrary Doppler spectrum shapes in general. It is found that the correlation values are based solely on the ICI-to-noise ratio. Moreover, the correlation values are very high for the residual ICI beyond the few dominant terms.

Secondly, to capitalize on the above high correlation to improve signal reception over fast varying channels, we consider performing simple blockwise whitening of the residual I+N before signal detection (i.e., equalization), where the whitener makes use of the ICI characteristics as found. Numerical results show that substantial gains can be achieved with this approach.

This chapter describes the system model and introduced this thesis organization.

In Chap. 2, we introduce some mobile channel characterization.

In Chap. 3, we find that, in a mobile time-varying channel, the residual ICI beyond several dominant terms had high normalized autocorrelation. We derive a rather precise closed-form approximation for the (unnormalized) autocorrelation function. As a result, a whitening transform for the residual ICI plus noise can be obtained based solely on the ICI-to-noise ratio.

In Chap. 4, we consider MLSE-type signal detection in ICI with blockwise whitening of the residual ICI plus noise. Simulations and SINR numerical analysis are provided.

In Chap. 5, we consider LMMSE signal detection with blockwise whitening of residual ICI plus noise. We present some simulation results based on 3×3 block whitening and three-sample equalization. The results show that a good tradeoff between complexity and performance could be achieved.

Finally, Chap. 6 gives an overall conclusion and describes the potential future

topics.



Chapter 2

Wireless Channel Characterization

2.1 Wireless Channel

In general, “channel” can be used to mean everything between the source and the receiver. There may be more than one path over which the signal can travel between the transmitter and receiver over the air. Various signals are sent from the transmitter antennas and the all paths before it reaches the receiver antennas are referred as channel. The wireless users communicate over the air and then there is significant interference over channels. The wireless channel could be a simple straight line (Line of Sight, LOS). It also may be interfered by other factors, such as multi-path effects, which are due to atmospheric scattering and reflections from buildings and other objects.

Before arriving at the receiving antenna, the transmitted signal follows many different paths, and these paths constitute the multipath radio propagation channel. The resulting signal strength will undergo large fluctuations. How to deal with fading and with interference over channel is a key issue for the design of communication systems. The time variation of the channel strengths due to the small-scale effect of

multipath effects, as well as larger-scale effects such as shadowing by obstacles and path loss by distance attenuation. Shadow fading reveals itself as an attenuation of the average signal power. Shadow fading is induced by obstacles (buildings, hills, etc.) between transmitter and receiver. The wireless users communicating over the air often encounters both types of fading: multipath fading superimposed on the slower fading. The channel impulse response in the complex-lowpass equivalent form is composed of two components,

$$h(\tau, t) = s(t) \times \tilde{c}(\tau, t) \quad (2.1)$$

where $s(t)$ denotes the shadow fading component and $\tilde{c}(\tau, t)$ denotes the multipath component. (2.1) means the multipath fading is superimposed on the shadow fading. It turns out that channels gains vary over multiple time-scales. At a fast time-scale, channels vary due to the multipath effects. At a slow time-scale, channels vary due to large-scale fading effects such as shadowing and path loss by distance attenuation. The duration of a shadow fade lasts for multiple seconds or minutes, and hence occurs at a much slower time-scale compared to multipath fading. Since the shadow fading is slow and is often compensated by power control, it may be regarded as quasi-static. Large-scale shadowing fading is often relevant to issues such as cell-site planning. Small-scale multipath fading is often relevant to the wireless communication systems design. For a given shadow fading component, the signal envelope is conditionally Rayleigh or Ricean distribution. If there is no LOS signal contribution to the receiver, the signal follows a Rayleigh distribution. If there is a LOS signal contribution to the receiver, the signal follows a Ricean distribution.

2.2 Multipath Fading

In a multipath channel, the transmitted signals arriving along different paths can have different attenuations and delays and they might be superimposed either constructively or destructively at the receiver. This is the phenomenon of multipath fading.

Two of the important multipath fading channels are the diffuse and discrete

channels [31]. Many realistic channels contain both diffuse and discrete properties. Those two properties often are separated for the purpose of channel modeling.

1. Diffuse multipath channel: The multipath signal paths are generated by a large number of unresolvable reflections. The Diffuse multipath fading might occur in an urban or a mountainous area. The signal envelope generated by lots unresolvable reflections is Rayleigh or Ricean distribution.

2. Discrete multipath channel: The multipath paths are made up of a few identifiable and resolvable components, which are reflected by hills or structures in open or rural areas. This results in a channel model with a finite number of multipath components.

2.2.1 Statistical Characterization of Multipath Channels

The multipath channels for both the diffuse and discrete effects have the following statistical characterization [31]:

1. Time spreading of the symbol duration in τ , which can be modeled as a set of discrete resolvable multipath components [31]: The channels effect is equivalent to filtering and band-limiting. A popular model for discrete multipath channels is the tapped-delay-line (TDL) channel model [33,34].

2. A time-variant channel behavior in t due to the motion of the receiver or the changing environment such as movements of reflectors or scatters: A popular channel model describing a time-variant behavior is the Jakes Doppler Spectrum.

2.2.2 Doubly Selective Channel Model

The doubly selective channel actually means the multipath channel with the time-variant behavior. Different time-variant and frequency selective fading channels may be simulated, depending on the settings of gain and time delay. They are shown in Fig. 2.1.

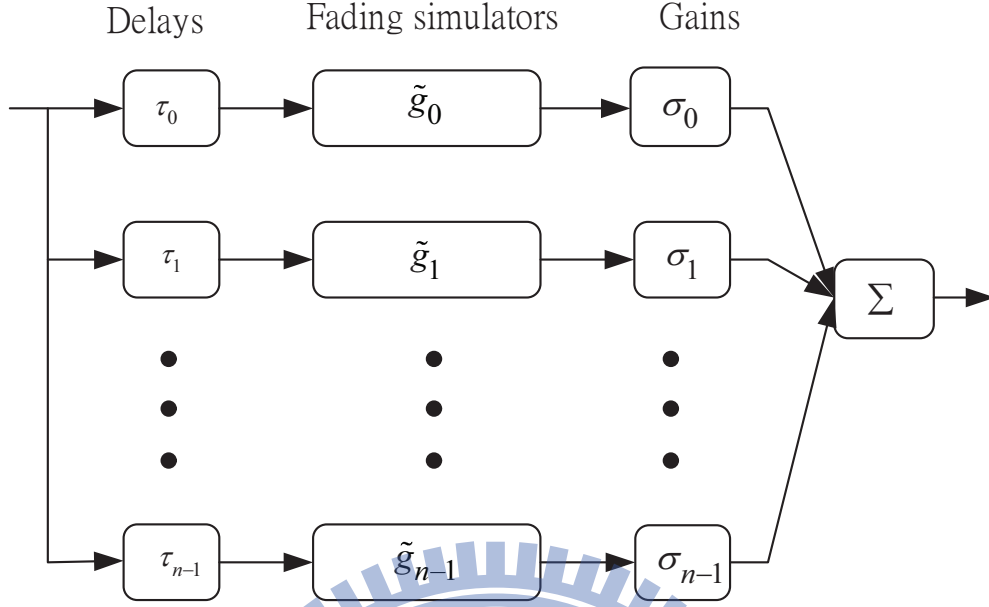


Figure 2.1: Frequency Selective Fading Channel Simulators.

2.3 Statistical Characterization of the Time-Variant Behavior

The components of the multipath fading received signal can be modeled by treating $\tilde{c}(\tau, t)$ as a random process in t . Since $\tilde{c}(\tau, t)$ arises from a large number of reflections and scattering, then by the central limit theorem, it can be modeled as a complex Gaussian process. In radio communications, the most common model describing flat fading in urban/suburban environments is Clarke's model [35].

At any time t , the probability density functions of the real and imaginary parts of $\tilde{c}(\tau, t)$ are Gaussian. If $\tilde{c}(\tau, t)$ has a zero mean, then the envelope $|\tilde{c}(\tau, t)| = r$ can be shown [36] to be Rayleigh-distributed, i.e. with probability density function (pdf):

$$p(r) = \frac{r}{\sigma^2} e^{-\frac{r^2}{2\sigma^2}} \quad (2.2)$$

where σ^2 is the time-average power of the received signal before envelope detection. If $\tilde{c}(\tau, t)$ has a nonzero mean, which implies there is a significant line-of-sight component present, can then be shown [36] to be Rician-distributed, i.e. with pdf:

$$p(r) = \frac{r}{\sigma^2} e^{-\frac{(r^2+A^2)}{2\sigma^2}} I_0\left(\frac{Ar}{\sigma^2}\right) \quad (2.3)$$

where A is the nonzero mean of and $I_0(\cdot)$ is the zero-order modified Bessel function of the first kind. In such a situation, random multipath components arriving at different angles are superimposed on a stationary dominant signal. A ratio $K = A^2/(2\sigma^2)$ is an indicator of the relative power in the faded and unfaded components. K is termed the Rician K-factor and completely specifies the Ricean distribution. As $K \gg 1$, and as the dominant path fades away, the Ricean distribution degenerates to a Rayleigh distribution.

2.4 Statistical Characterization: The WSSUS Model

A frequency-flat fading channel simulator needs to reproduce the Doppler spreading only, while a frequency-selective fading channel simulator should emulate both Doppler spreading and time spreading. In general, the time spreading and Doppler spreading are mutually related. However, most channel simulators treat the two spreading processes independently for simplicity.

Such simulators are said to follow the Wide-Sense Stationary Uncorrelated Scattering (WSSUS) assumption in [32]. In the sections below, common approaches are reviewed for separately simulating the Doppler spreading process and the time spreading process. A model for the multipath channel that includes both the variations in t and τ was introduced by Bello [32]. The time-varying channel $\tilde{c}(\tau, t)$ is modeled as a wide-sense stationary (WSS) random process in t with an autocorrelation function

$$R_{\tilde{c}}(\tau_1, \tau_2, \Delta t) = E[\tilde{c}^*(\tau_1, t)\tilde{c}(\tau_2, t + \Delta t)] \quad (2.4)$$

In most multipath channels, the attenuation and phase shift associated with different

delays may be uncorrelated. This is the uncorrelated scattering (US) assumption, which leads to

$$R_{\tilde{c}}(\tau_1, \tau_2, \Delta t) = R_{\tilde{c}}(\tau_1, \Delta t)\delta(\tau_2 - \tau_1) \quad (2.5)$$

The most important class of stochastic time-variant linear channel models is represented by models belonging to the WSS models as well as to the US models. These channel models with both the WSS and US assumptions are called WSSUS models (WSSUS, wide-sense stationary uncorrelated scattering). This autocorrelation function is denoted by $R_{\tilde{c}}(\Delta\tau, \Delta t)$, and

$$R_{\tilde{c}}(\Delta\tau, \Delta t) = E[\tilde{c}(\tau, t)\tilde{c}(\tau + \Delta\tau, t + \Delta t)] \quad (2.6)$$

Due to their simplicity, they are of great practical importance and are nowadays almost exclusively employed for modeling frequency-selective mobile radio channels.

2.5 The Time-Varying Channel

For mobile radio applications, the channel is time-varying because the motion between the transmitter and receiver results in propagation paths change. It should be noted that since the channel characteristics are dependent on the relative positions of the transmitter and receiver, time variance is equivalent to space variance. As mentioned previously, the time variation of the channel is characterized by the Doppler power spectrum. Although Doppler power spectrums apply to any time-variant model, for the sake of simplicity we present the commonly used Jakes model.

2.5.1 Jakes Doppler Spectrum

Jakes Doppler spectrum applies to time-varying channels. The so-called "Jakes" Doppler power spectrum model is due to Gans [37]. Gans analyzed the Doppler spectrum of time-varying channels by Clarke's model [35], which is also called the "classical model". Jakes Doppler spectrum follows the following assumptions [38,39]:

1. The radio waves propagate horizontally.

2. The ray arrival angles at receivers are uniformly distributed over $[-\pi, \pi]$.

3. The receiver's antenna is omnidirectional. The normalized Jakes Doppler spectrum is given by

$$S_j(f) = \frac{1}{\pi f_d \sqrt{1 - (f/f_d)^2}}, |f| \geq f_d \quad (2.7)$$

where f_d is the maximum Doppler shift. And the corresponding autocorrelation is then:

$$R_j(\tau) = J_0(2\pi f_d \tau) \quad (2.8)$$

where $J_0(z)$ is the Bessel function of the first kind of order 0. We will have the amplitude of the frequency response as

$$|H_j(f)| = \sqrt{S_j(f)} \quad (2.9)$$

2.5.2 Doppler Spreading Simulation

The Rayleigh or Rician fading simulators designed to ensure that the following two properties are approximately verified, Due to the Doppler spreading, its power spectrum is given by the Clarke model, or by any other specified spectrum. For simulated fading process, its envelope should be Rayleigh or Rician-distributed. Two popular methods are sum-of-sinusoids (SoS) simulators and filtered Gaussian noise (FGN) simulators [39].

1. Simulators by Summing of Sinusoids

Like Clarke's model, many sum of sinusoids simulators for fading channel have been proposed over the past three decades. Simulators by summing of sinusoids create the fading process by superposing several waves, each one being characterized by random amplitude, angle of arrival, and phase. As mention above, the resulting process of fading tends towards a Gaussian distribution due to the central limit theorem.

2. Simulators Filtering Gaussian Process with The Doppler Filters

A straightforward method of constructing simulators is to filter two independent white Gaussian noise with low-pass filters (Doppler filter). The Doppler filters $H(f)$ (impulse response) are to approximate the desired Doppler spectrum by eq(2.9). A complex Gaussian fading process with desired spectrums can be obtained by filtering with a Doppler filter. Both finite impulse response (FIR) filters and infinite impulse response (IIR) filters have been proposed as the Doppler filters. The filtering operation can be carried out in either the time domain or the frequency domain. A simple example was shown in [31] p.575.



Chapter 3

Autocorrelation of Residual Intercarrier Interference

In this chapter, we try to characterize this autocorrelation function of residual ICI plus noise from the viewpoint of signal detection. We derived a rather precise closed-form approximation for the (unnormalized) autocorrelation function. It is found that the correlation values are based solely on the ICI-to-noise ratio. Moreover, the correlation values are very high for the residual ICI beyond the few dominant terms.

The remainder of this chapter is organized as follows. Sec. 3.1 analyzes the correlation property of ICI. Sec. 3.2, we verify some key results above by considering multipath Rayleigh fading and simple Doppler frequency shift. Finally, Sec. 3.4 gives a summary.

3.1 Derivation of Autocorrelation of Residual ICI

Assume a signal detector (equalizer) able to handle $2K$ terms of nearest-neighbor ICI. We may partition the summation over k in (1.2) into an in-band and an out-of-band term as

$$Y_m = \sum_{k=m-K}^{m+K} \sum_{l=0}^{L-1} H_l^{(m-k)} e^{-j2\pi lk/N} X_k + \underbrace{\sum_{k \notin [m-K, m+K]} \sum_{l=0}^{L-1} H_l^{(m-k)} e^{-j2\pi lk/N} X_k}_{\triangleq c_{m,K}} + W_m, \quad (3.1)$$

where $c_{m,K}$ is the out-of-band term, i.e., residual ICI. Alternatively, using the notation of (1.6),

$$Y_m = \sum_{k=m-K}^{m+K} a_{m,k} X_k + c_{m,K} + W_m \quad (3.2)$$

where

$$c_{m,K} = \sum_{k \notin [m-K, m+K]} a_{m,k} X_k. \quad (3.3)$$

For large enough N , the residual ICI may be modeled as Gaussian by the central limit theorem.

It turns out that the analysis can be more conveniently carried out by way of the frequency spreading functions of the propagation paths than by way of $a_{m,k}$. Hence consider (3.1). From it, the autocorrelation of $c_{m,K}$ at lag r is given by

$$\begin{aligned} E[c_{m,K} c_{m+r,K}^*] &= E_s \times \sum_{\substack{k \notin [m-K, m+K] \\ \cup [m+r-K, m+r+K]}} \sum_{l=0}^{L-1} E[H_l^{(m-k)} H_l^{(m+r-k)*}] \\ &= E_s \times \sum_{k \notin [-K, K] \cup [-K-r, K-r]} \sum_{l=0}^{L-1} E[H_l^{(k)} H_l^{(k+r)*}] \end{aligned} \quad (3.4)$$

where E_s is the average transmitted symbol energy and we have assumed that X_k is white. Invoking (1.3) and (1.7), we get

$$E[c_{m,K} c_{m+r,K}^*] = \frac{E_s}{N^2} \sum_{l=0}^{L-1} \sum_{n=0}^{N-1} \sum_{n'=0}^{N-1} \sum_{\substack{k \notin [-K, +K] \\ \cup [-K-r, K-r]}} \sigma_l^2 r_l(n-n') e^{j2\pi[n'(k+r)-nk]/N}. \quad (3.5)$$

We show in the Sec. 3.3 that

$$E[c_{m,K}c_{m+r,K}^*] \approx 4\pi^2 T_{sa}^2 E_s \left(\sum_{l=0}^{L-1} \sigma_l^2 \sigma_{Dl}^2 \right) \rho(K, r, N) \quad (3.6)$$

where σ_{Dl}^2 is the mean-square Doppler spread of path l given by $\sigma_{Dl}^2 = \int_{-f_d}^{f_d} P_l(f) f^2 df$ and

$$\rho(K, r, N) = \sum_{k \notin [-K, K] \cup [-K-r, K-r]} \frac{1}{(1 - e^{-j2\pi k/N})(1 - e^{j2\pi(k+r)/N})}. \quad (3.7)$$

Note that

$$\begin{aligned} \rho(K, r, N) &= \underbrace{\sum_{k \in [0, N-1] \setminus \{0, -r\}} \frac{1}{(1 - e^{-j2\pi k/N})(1 - e^{j2\pi(k+r)/N})}}_{\triangleq \rho_0(r, N)} \\ &\quad - \underbrace{\sum_{k \in [-K, K] \cup [-K-r, K-r] \setminus \{0, -r\}} \frac{1}{(1 - e^{-j2\pi k/N})(1 - e^{j2\pi(k+r)/N})}}_{\triangleq \rho_1(K, r, N)}, \end{aligned} \quad (3.8)$$

where the exclusion of 0 and $-r$ from both ranges of summation is to skip over the points of singularity where the summands are null anyway. Note further that $-1/(1 - e^{-j2\pi k/N})$ and $-1/(1 - e^{-j2\pi(k+r)/N})$ (as sequences in k) are the DFTs of $[n - (N-1)/2]/N$ and $e^{-j2\pi rn/N}[n - (N-1)/2]/N$ (as sequences in n), respectively. Hence, with Parseval's theorem we get

$$\rho_0(r, N) = \frac{1}{N} \sum_{n=0}^{N-1} \left(n - \frac{N-1}{2} \right)^2 e^{j2\pi rn/N} = \begin{cases} \frac{N^2-1}{12}, & r = 0, \\ \frac{-2}{(1-e^{j2\pi r/N})^2}, & r \neq 0. \end{cases} \quad (3.9)$$

For $\rho_1(K, r, N)$, we have

$$\rho_1(K, r, N) = \rho_1^*(K, -r, N), \quad (3.10)$$

i.e., it is conjugate symmetric in r . Moreover, the summands in the last summation in (3.8) are symmetric over the range of summation. But the range of summation does not allow us to obtain a compact expression for $\rho_1(K, r, N)$ as that for $\rho_0(r, N)$.

As mentioned, the proposed receiver will whiten the residual I+N before equalization. Here we make some observations of the properties of the normalized autocorrelation of residual ICI, i.e., $E[c_{m,K}c_{m+r,K}^*]/E[|c_{m,K}|^2]$, that are relevant to whitener design and performance. For this, note from (3.6) that $E[c_{m,K}c_{m+r,K}^*]/E[|c_{m,K}|^2]$

depends only on K and N through $\rho(K, r, N)$; the other factors cancel out. Thus this normalized autocorrelation is independent of the average transmitted symbol energy E_s and the sample period T_{sa} . More interestingly, it is also independent of the power-delay profile (PDP) of the channel (i.e., σ_l^2 vs. l) and the Doppler PSD $P_l(f)$ of each path. While the independence of the normalized autocorrelation on the average transmitted symbol energy may be intuitively expected, its independence of the sample period, the PDP, and the Doppler PSDs of channel paths appears somewhat surprising.

Moreover, the normalized autocorrelation is also substantially independent of the DFT size N . To see this, note that for complexity reason, in a practical receiver both the whitener and the equalizer are likely short. A short equalizer implies a small K and a short whitener implies a small range of r over which the normalized autocorrelation needs to be computed. Hence, when N is large, the exponential functions in the above summations for $\rho_0(r, N)$ and $\rho_1(K, r, N)$ can all be well approximated with the first two terms of their respective power series expansion (i.e., $e^x \approx 1 + x$ when $|x| \ll 1$). As a result, we have

$$\rho(K, r, N) = \rho_0(r, N) - \rho_1(K, r, N) \quad (3.11)$$

where

$$\rho_0(r, N) \approx \begin{cases} \frac{N^2}{12}, & r = 0, \\ \frac{N^2}{2\pi^2 r^2}, & r \neq 0, \end{cases} \quad (3.12)$$

$$\rho_1(K, r, N) \approx \sum_{k \in [-K, K] \cup [-K-r, K-r] \setminus \{0, -r\}} \frac{N^2}{4\pi^2 k(k+r)}. \quad (3.13)$$

Thus the normalized autocorrelation, being essentially given by $\rho(K, r, N)/\rho(K, 0, N)$, is substantially independent of the DFT size N .

The rules are given below.

Property 1

Assume a receiver partition the frequency channel matrix with band width K into an in-band and an out-of-band term and is out-of-band term at m -th subcarrier.

The normalized autocorrelation of $c_{m,K}$ at lag r is given by

$$\frac{E[c_{m,K}c_{m+r,K}^*]}{E[|c_{m,K}|^2]} \approx \frac{1/r^2 - \sum_{k \in [-K,K] \cup [-K-r,K-r] \setminus \{0,-r\}} 1/2k(k+r)}{\pi^2/6 - \sum_{k=1}^K 1/k^2}, \quad (3.14)$$

that will approximate to a constant on condition that K, r are given.

Although the above observations concern ICI only, it is straightforward to extend them to the sum of ICI and AWGN channel noise.

Property 2

The normalized autocorrelation of Z_m (i.e. $c_{m,K} + W_m$) at lag r is given by

$$\frac{E[Z_m Z_{m+r}^*]}{E[|Z_m|^2]} \approx \frac{1/r^2 - \sum_{k \in [-K,K] \cup [-K-r,K-r] \setminus \{0,-r\}} 1/2k(k+r)}{\pi^2/6 - \sum_{k=1}^K 1/k^2} \frac{1}{1 + \frac{E[|W_m|^2]}{E[|c_{m,K}|^2]}} \quad (3.15)$$

that will approximate to a function only depends on $\frac{E[|W_m|^2]}{E[|c_{m,K}|^2]}$ with K, r given.

In particular, the resulting whitening filter and its performance can also disregard a variety of system parameters and channel conditions, including the DFT size, the sample period, the system bandwidth (which is approximately proportional to the inverse of the sample period), the OFDM symbol period NT_{sa} , the channel PDP, and the Doppler PSDs of the channel paths. They only depend on the ICI-to-noise power ratio (INR) at the receiver.

As a result, a whitener parameterized on receiver INR can be designed for all operating conditions, which is advantageous for practical system implementation. (The estimation of ICI and noise powers is outside the scope of the present work. Some applicable methods have been proposed in the literature, e.g., [11] for ICI power and [12] for noise power.)

The whitener performance can be understood to a substantial extent by examining the above approximation to the normalized autocorrelation $E[c_{m,K}c_{m+r,K}^*]/E[|c_{m,K}|^2]$. We leave a detailed study along this vein to potential future work. For now, we shall be content with a first-order understanding by a look at its value at lag $r = 1$. A

large value indicates that whitening can effectively lower the residual ICI. For this, we see from the above approximation (after some straightforward algebra) that

$$\frac{E[c_{m,K}c_{m+1,K}^*]}{E[|c_{m,K}|^2]} \approx \frac{\rho(K, 1, N)}{\rho(K, 0, N)} \approx \frac{1 - \sum_{k=1}^K 1/[k(k+1)]}{\pi^2/6 - \sum_{k=1}^K 1/k^2} = \frac{1/(K+1)}{\pi^2/6 - \sum_{k=1}^K 1/k^2}. \quad (3.16)$$

For example, its values for $K = 0-3$ are, respectively, 0.6079, 0.7753, 0.8440, and 0.8808, which are substantial indeed.

As a side remark that will be of use later, we note the following properties from (3.6) and (3.11).

Property 3

The total ICI power $E[|c_{m,0}|^2]$ can be approximated as

$$\sigma_{c0}^2 \triangleq E[|c_{m,0}|^2] \approx 4\pi^2 T_{sa}^2 E_s \left(\sum_{l=0}^{L-1} \sigma_l^2 \sigma_{Dl}^2 \right) \rho(0, 0, N) \approx \frac{E_s}{12} (2\pi T_{sa} N)^2 \left(\sum_{l=0}^{L-1} \sigma_l^2 \sigma_{Dl}^2 \right), \quad (3.17)$$

which is in essence the upper bound derived in [11]. Moreover, we have an approximation to the partial ICI power beyond the $2K$ central terms.

Property 4

The total ICI power $E[|c_{m,K}|^2]$ can be approximated as

$$\sigma_{cK}^2 \triangleq E[|c_{m,K}|^2] \approx 4\pi^2 T_{sa}^2 E_s \left(\sum_{l=0}^{L-1} \sigma_l^2 \sigma_{Dl}^2 \right) \rho(K, 0, N) \approx \sigma_{c0}^2 \left(1 - \frac{6}{\pi^2} \sum_{k=1}^K \frac{1}{k^2} \right). \quad (3.18)$$

In the following section, we provide some numerical examples to verify the above results on ICI correlation. Then, in the next section, we consider how to incorporate a whitener for residual ICI plus noise in the receiver.

3.2 Numerical Examples

In this section, we verify some key results above by considering two very different channel conditions: multipath Rayleigh fading and simple Doppler frequency shift.

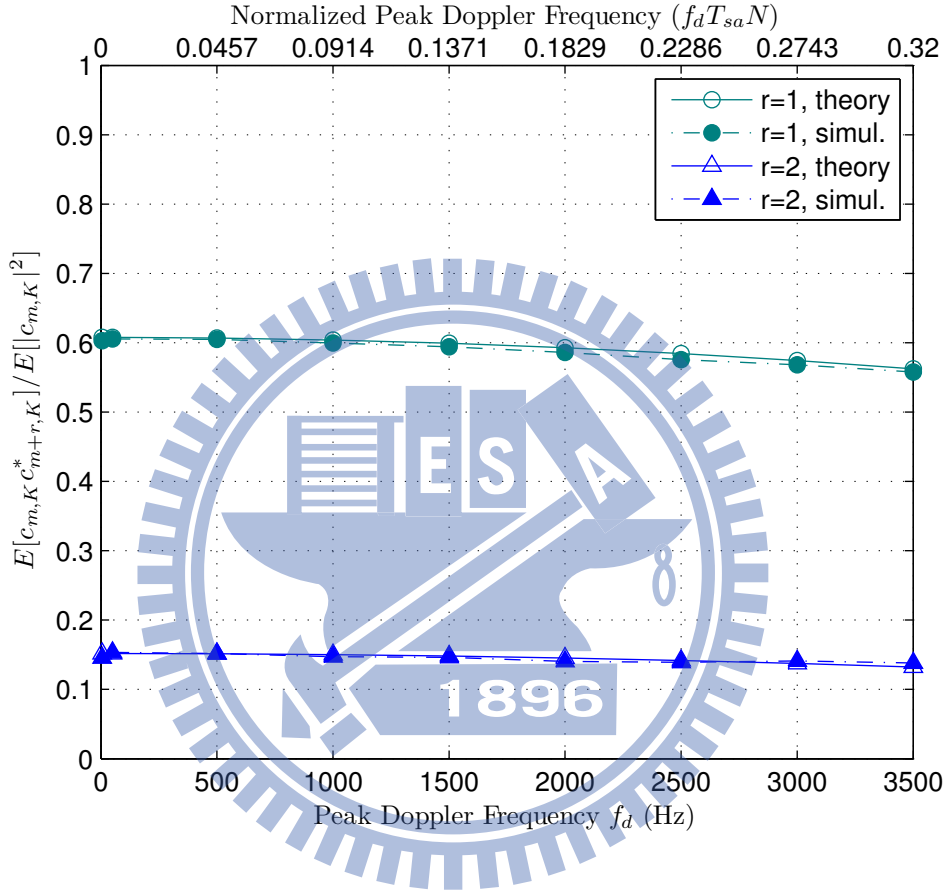


Figure 3.1: Normalized autocorrelation of residual ICI over multipath Rayleigh fading channel at $K = 0$, with $N = 128$ and $T_{sa} = 714$ ns. The first-order approximation (3.11)–(3.13) yields 0.6079 for $r = 1$ and 0.1520 for $r = 2$, which are quite accurate at low f_d values.

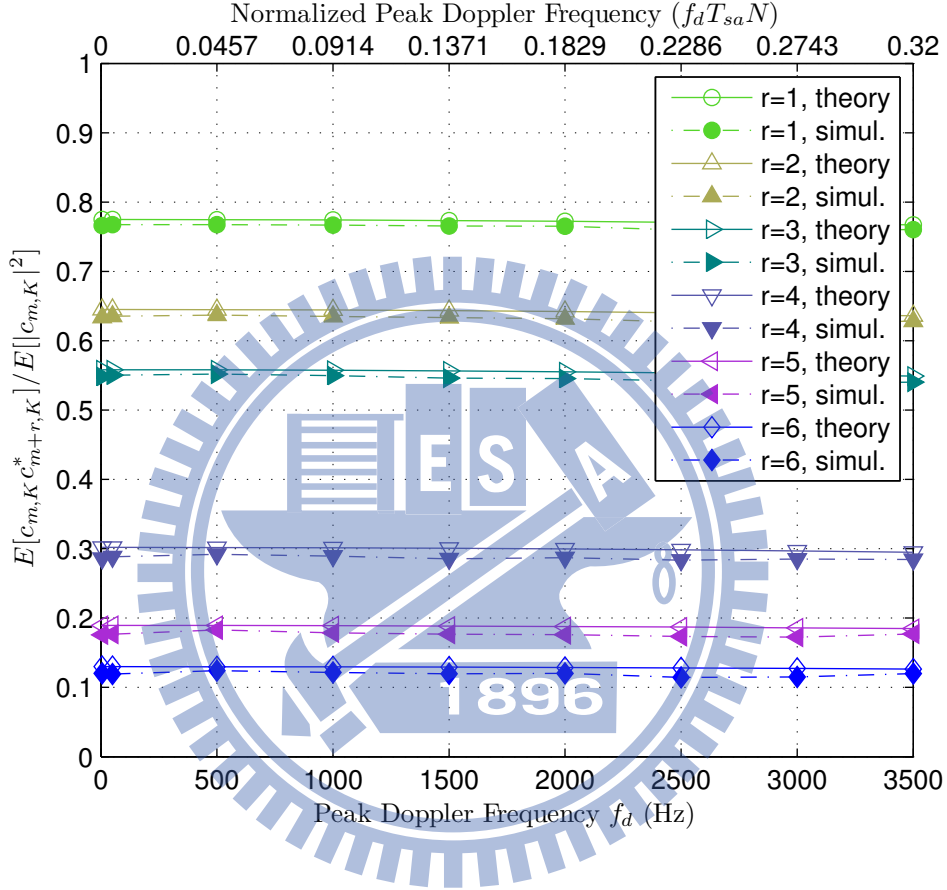


Figure 3.2: Normalized autocorrelation of residual ICI over multipath Rayleigh fading channel at $K = 1$, with $N = 128$ and $T_{sa} = 714$ ns. The first-order approximation (3.11)–(3.13) yields 0.7753, 0.6461, 0.5599, 0.3036, 0.1912, and 0.1317, for $r = 1$ –6, respectively, which are quite accurate.

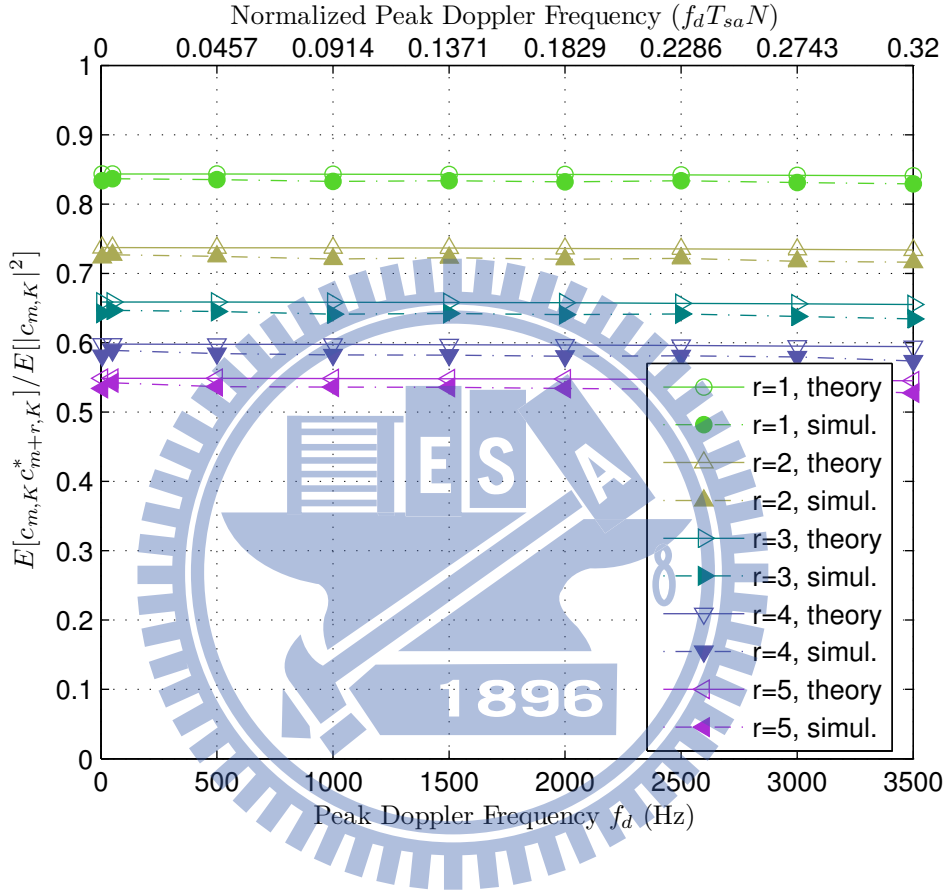


Figure 3.3: Normalized autocorrelation of residual ICI over multipath Rayleigh fading channel at $K = 2$, with $N = 128$ and $T_{sa} = 714$ ns. The first-order approximation (3.11)–(3.13) yields 0.8440, 0.7358, 0.6612, 0.6014, and 0.5534, for $r = 1$ –5, respectively, which are quite accurate.

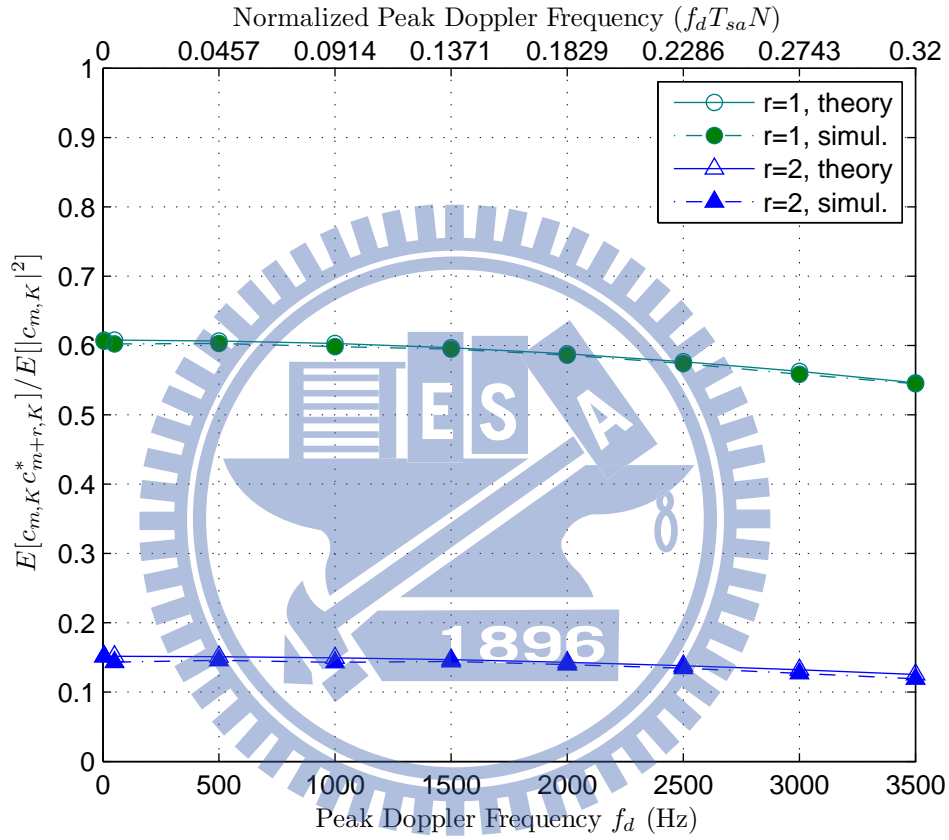


Figure 3.4: Normalized autocorrelation of residual ICI over one-Doppler-line channel at $K = 0$, with $N = 128$ and $T_{sa} = 714$ ns.

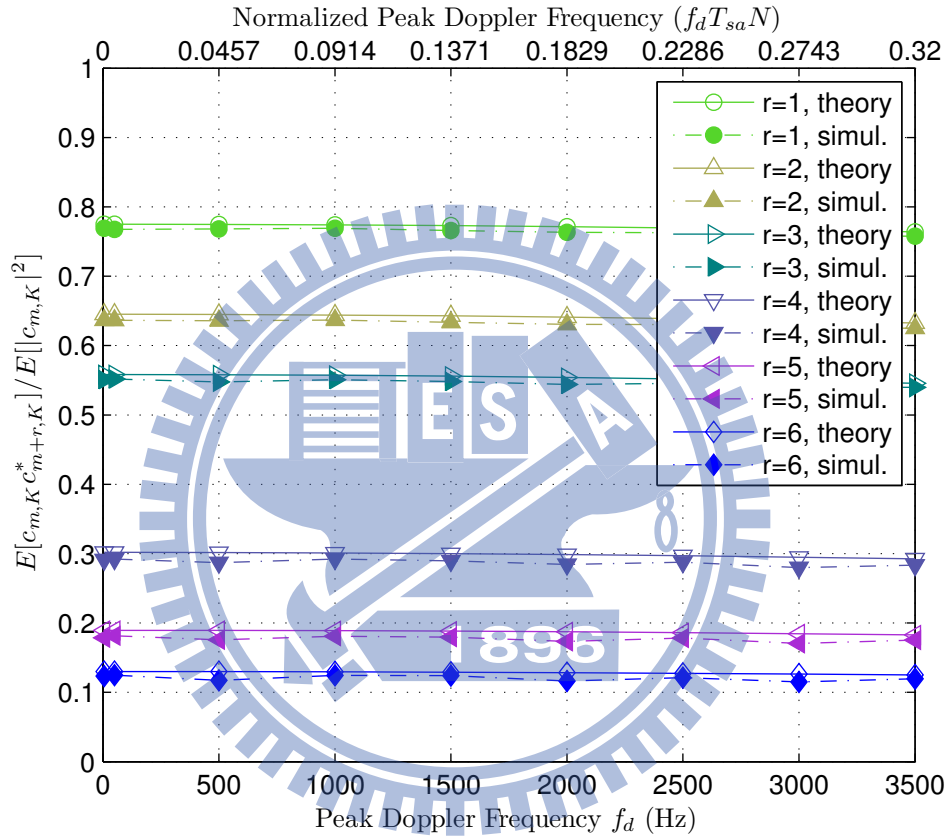


Figure 3.5: Normalized autocorrelation of residual ICI over one-Doppler-line channel at $K = 1$, with $N = 128$ and $T_{sa} = 714$ ns.

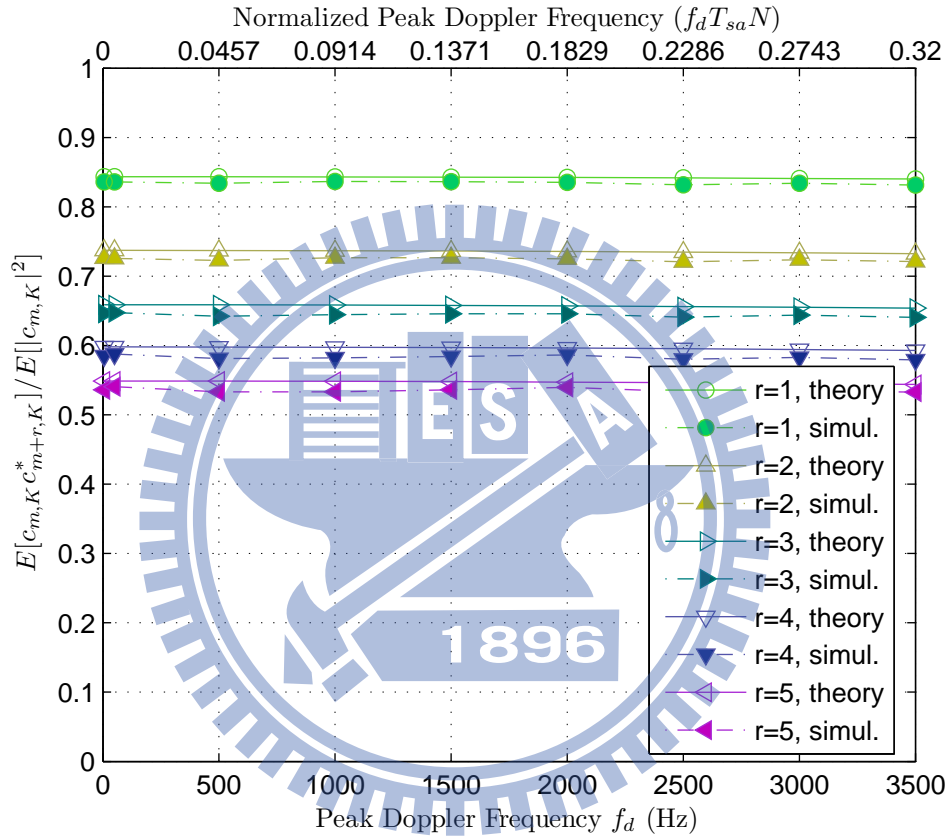


Figure 3.6: Normalized autocorrelation of residual ICI over one-Doppler-line channel at $K = 2$, with $N = 128$ and $T_{sa} = 714$ ns.

First, consider a multipath channel having the COST 207 6-tap Typical Urban (TU6) PDP as shown in Table 4.1 [13, p. 94]. Let the paths be subject to Rayleigh fading with the same peak Doppler frequency f_d , so that $r_l(q) = J_0(2\pi f_d T_{sa} q)$ for all l , where $J_0(\cdot)$ denotes the zeroth-order Bessel function of the first kind [10]. Let the OFDM system have $N = 128$, subcarrier spacing $f_s = 10.94$ kHz, and sampling period $T_{sa} = 1/(Nf_s) = 714$ ns, which are some of the Mobile WiMAX parameters [1].

Figs. 3.1–3.3 illustrate the normalized autocorrelation of the residual ICI for $K = 0$ –2, respectively, where the theoretical values are calculated using (3.5). As points of reference, note that a peak Doppler frequency of 1 kHz corresponds to a 180 km/h mobile speed at a 6 GHz carrier frequency, or a 540 km/h mobile speed at a 2 GHz carrier frequency. Figs. 3.1–3.3 show that the theory and the simulation results agree well up to very large Doppler spreads. In addition, they also show that, for given lag r , the normalized autocorrelation increases with K . The last fact can be understood by examining (3.3): as K increases, the residual ICI $c_{m,K}$ is composed of the sum of increasingly fewer terms with generally smaller magnitudes, which naturally leads to higher normalized autocorrelation.

Next, consider a channel with a one-line Doppler PSD equal to $\delta(f - f_d)$; in other words, the channel simply effects a frequency offset of f_d . The temporal autocorrelation of the CIR is given by $r_l(q) = \exp(j2\pi f_d T_{sa} q)$. It turns out that the normalized autocorrelation of residual ICI is very similar to that obtained for the previous example, as the theory predicts. Figs. 3.4–3.6 illustrate the corresponding normalized autocorrelation of the residual ICI for $K = 0$ –2, respectively. They are very similar to Figs. 3.1–3.3, as the theory predicts.

Looking backwards from the one-Doppler-line example to the earlier analysis in this Section 3.1, we find that this example also provides an alternative way of interpreting the earlier analytical results. Specifically, an arbitrary Doppler PSD can be considered as composed of a (possibly infinite) number of line PSDs. Hence the autocorrelation of residual ICI associated with an arbitrary Doppler PSD may be obtained as a linear combination of the autocorrelation associated with a line

PSD as

$$E[c_{m,K}c_{m+r,K}^*]|_{any_shape} = \sum_{l=0}^{L-1} \sigma_l^2 \int_{-f_d}^{f_d} P_l(f) E[c_{m,K}c_{m+r,K}^*]|_{line,f} df \quad (3.19)$$

where $E[c_{m,K}c_{m+r,K}^*]|_{any_shape}$ denotes the autocorrelation of residual ICI associated with a multipath channel of arbitrary Doppler PSD and $E[c_{m,K}c_{m+r,K}^*]|_{line,f}$ that associated with a line Doppler PSD corresponding to a Doppler frequency f . As we have verified now (through Figs. 3.4–3.6, for example) that

$$\frac{E[c_{m,K}c_{m+r,K}^*]|_{line,f_d}}{E[c_{m,K}c_{m,K}^*]|_{line,f_d}} \approx \frac{\rho(K, r, N)}{\rho(K, 0, N)}, \quad (3.20)$$

substituting it into (3.19) yields

$$\begin{aligned} E[c_{m,K}c_{m+r,K}^*]|_{any_shape} &\approx \frac{\rho(K, r, N)}{\rho(K, 0, N)} \times \sum_{l=0}^{L-1} \sigma_l^2 \int_{-f_d}^{f_d} P_l(f) E[c_{m,K}c_{m,K}^*]|_{line,f} df \\ &= \frac{\rho(K, r, N)}{\rho(K, 0, N)} \times E[c_{m,K}c_{m,K}^*]|_{any_shape}. \end{aligned} \quad (3.21)$$

In other words, since the single-Doppler-line channel shows substantial invariance of the normalized residual ICI autocorrelation over a large range of operating conditions (as we have seen in the last example), it follows that a channel with any Doppler PSD has a similar property.

In summary, we have confirmed that the normalized autocorrelation of the residual ICI is quite insensitive to various system parameters and channel conditions. To lower the error floor, therefore, a whitening filter for the residual ICI plus noise can be designed without regard to these system parameters and channel conditions. Such a fixed design can lead to low implementation complexity and robust performance.

3.3 Derivation of (3.6) and Some Related Comments

Equation (3.5) gives

$$E[c_{m,K}c_{m+r,K}^*] = \frac{E_s}{N^2} \sum_{l=0}^{L-1} \sum_{n=0}^{N-1} \sum_{n'=0}^{N-1} \sum_{k \notin [-K,+K] \cup [-K-r,K-r]} \sigma_l^2 r_l(n-n') e^{j2\pi[n'(k+r)-nk]/N}.$$

Substituting the inverse Fourier transform relation in (1.8) into the right-hand side (RHS) of (3.5), we get

$$E[c_{m,K}c_{m+r,K}^*] = \frac{E_s}{N^2} \sum_{l=0}^{L-1} \sum_{n=0}^{N-1} \sum_{n'=0}^{N-1} \sum_{k \notin [-K,+K] \cup [-K-r,K-r]} \sigma_l^2 \cdot \int_{-f_d}^{f_d} P_l(f) \{ \cos[2\pi f T_{sa}(n-n')] + j \sin[2\pi f T_{sa}(n-n')] \} df \cdot e^{j2\pi[n'(k+r)-nk]/N}. \quad (3.22)$$

Let ξ denote the quantity that collects all the terms associated with $\sin[2\pi f T_{sa}(n-n')]$. That is,

$$\xi = \frac{E_s}{N^2} \sum_{l=0}^{L-1} \sigma_l^2 \int_{-f_d}^{f_d} df P_l(f) \sum_{n=0}^{N-1} \sum_{n'=0}^{N-1} \sum_{k \notin [-K,+K] \cup [-K-r,K-r]} j \sin[2\pi f T_{sa}(n-n')] e^{j2\pi[n'(k+r)-nk]/N}. \quad (3.23)$$

Consider the inner triple sum and denote it by χ . By substituting the variables n , n' , and k with ν' , ν , and $-(\kappa+r)$, respectively, we get, after some straightforward algebra,

$$\chi = \sum_{\nu=0}^{N-1} \sum_{\nu'=0}^{N-1} \sum_{\kappa \notin [-K,+K] \cup [-K-r,K-r]} -j \sin[2\pi f T_{sa}(\nu-\nu')] e^{j2\pi[\nu'(\kappa+r)-\nu\kappa]/N}. \quad (3.24)$$

A comparison with the inner triple sum in (3.23) shows that $\chi = -\chi$, which implies $\chi = 0$ and thus $\xi = 0$. Therefore, only the cosine terms remain in $E[c_{m,K}c_{m+r,K}^*]$. Approximating the cosine function by taking its power series expansion and retaining

only up to the second-order term as $\cos x \approx 1 - x^2/2$, we get

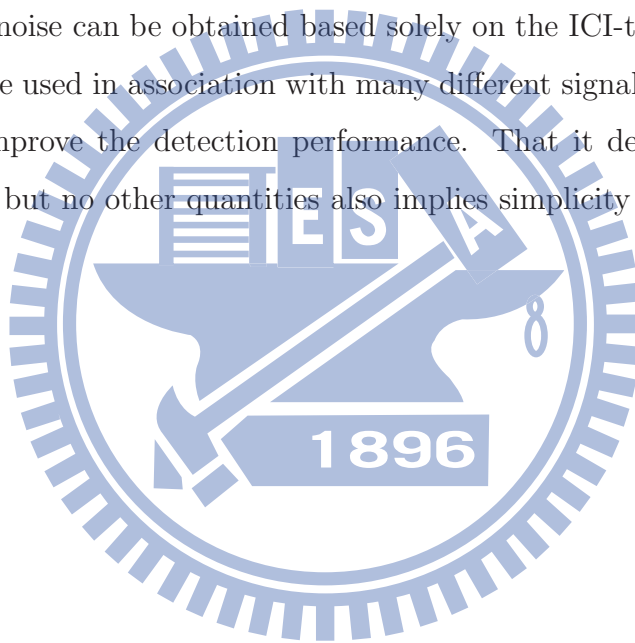
$$\begin{aligned}
& E[c_{m,K} c_{m+r,K}^*] \\
& \approx \frac{E_s}{N^2} \sum_{l=0}^{L-1} \sigma_l^2 \int_{-f_d}^{f_d} P_l(f) df \sum_{k \notin [-K,K] \cup [-K-r, K-r]} \underbrace{\sum_{n=0}^{N-1} e^{-j2\pi nk/N}}_{=0} \underbrace{\sum_{n'=0}^{N-1} e^{j2\pi n'(k+r)/N}}_{=0} \\
& \quad - \frac{E_s}{2N^2} \sum_{l=0}^{L-1} \sigma_l^2 \int_{-f_d}^{f_d} P_l(f) (2\pi f T_{sa})^2 df \sum_{k \notin [-K,K] \cup [-K-r, K-r]} \left[\sum_{n=0}^{N-1} n^2 e^{-j2\pi nk/N} \underbrace{\sum_{n'=0}^{N-1} e^{j2\pi n'(k+r)/N}}_{=0} \right. \\
& \quad \left. + \underbrace{\sum_{n=0}^{N-1} e^{-j2\pi nk/N}}_{=0} \sum_{n'=0}^{N-1} n'^2 e^{j2\pi n'(k+r)/N} - 2 \sum_{n=0}^{N-1} n e^{-j2\pi nk/N} \sum_{n'=0}^{N-1} n' e^{j2\pi n'(k+r)/N} \right] \\
& = 4\pi^2 T_{sa}^2 E_s \sum_{l=0}^{L-1} \sigma_l^2 \int_{-f_d}^{f_d} P_l(f) f^2 df \sum_{k \notin [-K,K] \cup [-K-r, K-r]} \frac{1}{(1 - e^{-j2\pi k/N})(1 - e^{j2\pi(k+r)/N})}. \quad (3.25)
\end{aligned}$$

In fact, the above second-order approximation to cosine function is tantamount to assuming linearly time-varying paths in the CIR. To see it, let $h_l(t)$ denote the continuous-time waveform of the l th path of the CIR (of which $h_{n,l}$ is a sampled version) and let $h'_l(t)$ be its time-derivative. Then by a well-known relation between the time-derivative of a stochastic process and its PSD, we have $4\pi^2 \sigma_l^2 \int P_l(f) f^2 df = E[|\overline{h'_l(t)}|^2]$ [20, Table 7.5-1]. Therefore, if we approximate the channel by one whose l th path response varies linearly with time in some period with its slope equal to $\left[\overline{|\overline{h'_l(t)}|^2}\right]^{1/2}$ in magnitude (where the overline in the brackets denotes time average over this period), then the autocorrelation of residual ICI of the approximating channel would be exactly that obtained above, without approximation. In this sense, the second-order approximation to cosine function above is tantamount to assuming linearly time-varying paths in the CIR.

Numerical examples in Section 3.1 show that the ensuing approximation to the autocorrelation of the residual ICI is rather accurate even under a relatively large peak Doppler shift.

3.4 Summary of Results

We found that, in a mobile time-varying channel, the residual ICI beyond several dominant terms had high normalized autocorrelation. We derived a rather precise closed-form approximation for the (unnormalized) autocorrelation function. It turns out that, up to a rather high peak Doppler frequency, the normalized autocorrelation was not sensitive to a variety of system parameters and channel conditions, including the DFT size, the sample period, the system bandwidth, the OFDM symbol period, the average transmitted symbol energy, the multipath channel profile, and the Doppler PSDs of the channel paths. As a result, a whitening transform for the residual ICI plus noise can be obtained based solely on the ICI-to-noise ratio. Such a transform can be used in association with many different signal detection schemes to significantly improve the detection performance. That it depends only on the ICI-to-noise ratio but no other quantities also implies simplicity and robustness.



Chapter 4

MLSE Detection with Whitening of Residual ICI Plus Noise

In Sec. 4.1, we considered MLSE-type signal detection with blockwise whitening of the residual ICI plus noise. Simulations showed that the proposed technique could lower the ICI induced error floor by several orders of magnitude in MLSE that addressed a few dominant ICI terms.

To capitalize on the above high correlation to improve signal reception over fast varying channels, In Sec. 4.4, we consider performing simple blockwise whitening of the residual I+N before signal detection (i.e., equalization), where the whitener makes use of the ICI characteristics as found. Numerical analysis of SINR also confirms that substantial gains can be achieved with this approach. The chapter is organized as follows.

The remainder of this chapter is organized as follows. Sec. 4.2, we presents complexity analysis of proposed method. Sec. 4.3 presents some simulation results on signal detection performance. Sec. 4.4 explores how signal detection performance depends on whitener parameter setting. Finally, Sec. 4.5 gives a summary.

4.1 MLSE Detection with Whitening of Residual ICI Plus Noise

As indicated, we propose to whiten the residual ICI plus noise in signal detection. This can be applied to many detection methods, including MMSE, iterative MMSE, decision-feedback equalization (DFE), MLSE, etc., providing a wide range of tradeoff between complexity and performance. In this chapter, we consider an MLSE-based technique both to illustrate how such whitening can be carried out and to demonstrate its benefit. For simplicity, rather than performing whitening over a complete sequence, we do blockwise whitening over windows of size $2q + 1$ where q may or may not be equal to K . The details are as follows.

Consider a vector of $2q + 1$ frequency-domain signal samples centered at sample m :

$$\mathbf{y}_m = [Y_{m-q} \cdots Y_m \cdots Y_{m+q}]' = \mathbf{H}_m \mathbf{x}_m + \mathbf{z}_m \quad (4.1)$$

where $\mathbf{x}_m = [X_{m-p} \cdots X_m \cdots X_{m+p}]'$ for some integer p , \mathbf{H}_m is a $(2q + 1) \times (2p + 1)$ submatrix of \mathbf{H} of bandwidth K , and \mathbf{z}_m collects all the right-hand-side (RHS) terms in (1.2) (or (1.4)) associated with Y_k , $m - q \leq k \leq m + q$, that do not appear in $\mathbf{H}_m \mathbf{x}_m$. The elements of \mathbf{z}_m include both residual ICI and channel noise. To avoid clogging the mathematical expressions with details, we have omitted explicit indexing of various quantities in (4.1) with the parameters K , p , and q , understanding that their dimensions and contents depend on these parameters. As an example, with the set of parameters $\{K = 1, q = 1, p = 2\}$ we have

$$\mathbf{H}_m = \begin{bmatrix} a_{m-1,m-2} & a_{m-1,m-1} & a_{m-1,m} & 0 & 0 \\ 0 & a_{m,m-1} & a_{m,m} & a_{m,m+1} & 0 \\ 0 & 0 & a_{m+1,m} & a_{m+1,m+1} & a_{m+1,m+2} \end{bmatrix} \quad (4.2)$$

whereas with $\{K = 1, q = 1, p = 1\}$,

$$\mathbf{H}_m = \begin{bmatrix} a_{m-1,m-1} & a_{m-1,m} & 0 \\ a_{m,m-1} & a_{m,m} & a_{m,m+1} \\ 0 & a_{m+1,m} & a_{m+1,m+1} \end{bmatrix}. \quad (4.3)$$

Let $\mathbf{K}_z = E[\mathbf{z}_m \mathbf{z}_m^H]$, i.e., the covariance matrix of \mathbf{z}_m , where superscript H stands for Hermitian transpose. The aforesaid blockwise whitening of residual ICI plus noise \mathbf{z}_m is given by

$$\tilde{\mathbf{y}}_m \triangleq \mathbf{K}_z^{-\frac{1}{2}} \mathbf{y}_m = \underbrace{\mathbf{K}_z^{-\frac{1}{2}} \mathbf{H}_m}_{\triangleq \tilde{\mathbf{H}}_m} \mathbf{x}_m + \underbrace{\mathbf{K}_z^{-\frac{1}{2}} \mathbf{z}_m}_{\triangleq \tilde{\mathbf{z}}_m} \quad (4.4)$$

where $\mathbf{K}_z^{-\frac{1}{2}}$ may be defined in more than one way. One choice is to let $\mathbf{K}_z^{-\frac{1}{2}} = \mathbf{U} \mathbf{\Lambda}^{-\frac{1}{2}} \mathbf{U}^H$ where \mathbf{U} is the matrix of orthonormal eigenvectors of \mathbf{K}_z and $\mathbf{\Lambda}$ is the diagonal matrix of corresponding eigenvalues of \mathbf{K}_z .

If block-by-block signal detection were desired, then the ML criterion would result in the detection rule $\hat{\mathbf{x}}_m = \arg \min_{\mathbf{x}_m} \|\tilde{\mathbf{y}}_m - \tilde{\mathbf{H}}_m \mathbf{x}_m\|^2$. As stated, we consider MLSE-based detection in this chapter.

In developing the MLSE-based detection method, we treat $\tilde{\mathbf{z}}_m$, $m = 0, \dots, N-1$, as if they were mutually independent, even though this may at best be only nearly so. Then the probability density function of the received sequence conditioned on the transmitted sequence would be

$$f(\tilde{\mathbf{y}}_0, \tilde{\mathbf{y}}_1, \dots, \tilde{\mathbf{y}}_{N-1} | \mathbf{x}_0, \mathbf{x}_1, \dots, \mathbf{x}_{N-1}) = f(\tilde{\mathbf{z}}_0, \tilde{\mathbf{z}}_1, \dots, \tilde{\mathbf{z}}_{N-1}) = \prod_{n=0}^{N-1} f(\tilde{\mathbf{z}}_n). \quad (4.5)$$

As a result, the recursive progression of the log-likelihood values, i.e.,

$$\Lambda_k \triangleq \log f(\tilde{\mathbf{z}}_0, \tilde{\mathbf{z}}_1, \dots, \tilde{\mathbf{z}}_k) = \Lambda_{k-1} + \log f(\tilde{\mathbf{y}}_k - \tilde{\mathbf{H}}_k \mathbf{x}_k), \quad k = 1, \dots, N-1, \quad (4.6)$$

leads to a standard Viterbi algorithm. Disregarding some common terms that do not affect sequence detection, in the Viterbi algorithm we may use $\|\tilde{\mathbf{y}}_k - \tilde{\mathbf{H}}_k \mathbf{x}_k\|^2$ as the branch metric instead of $\log f(\tilde{\mathbf{y}}_k - \tilde{\mathbf{H}}_k \mathbf{x}_k)$. Fig. 4.1 illustrates the trellis structure of the MLSE detector for $p = 1$ under QPSK modulation. A tradeoff between complexity and performance can be achieved by different choices of the three parameters K , q , and p , where p determines the number of states in each trellis stage and the three parameters jointly affect the branch metric structure in the trellis and the autocorrelation structure of the residual ICI (and thereby the whitener behavior).

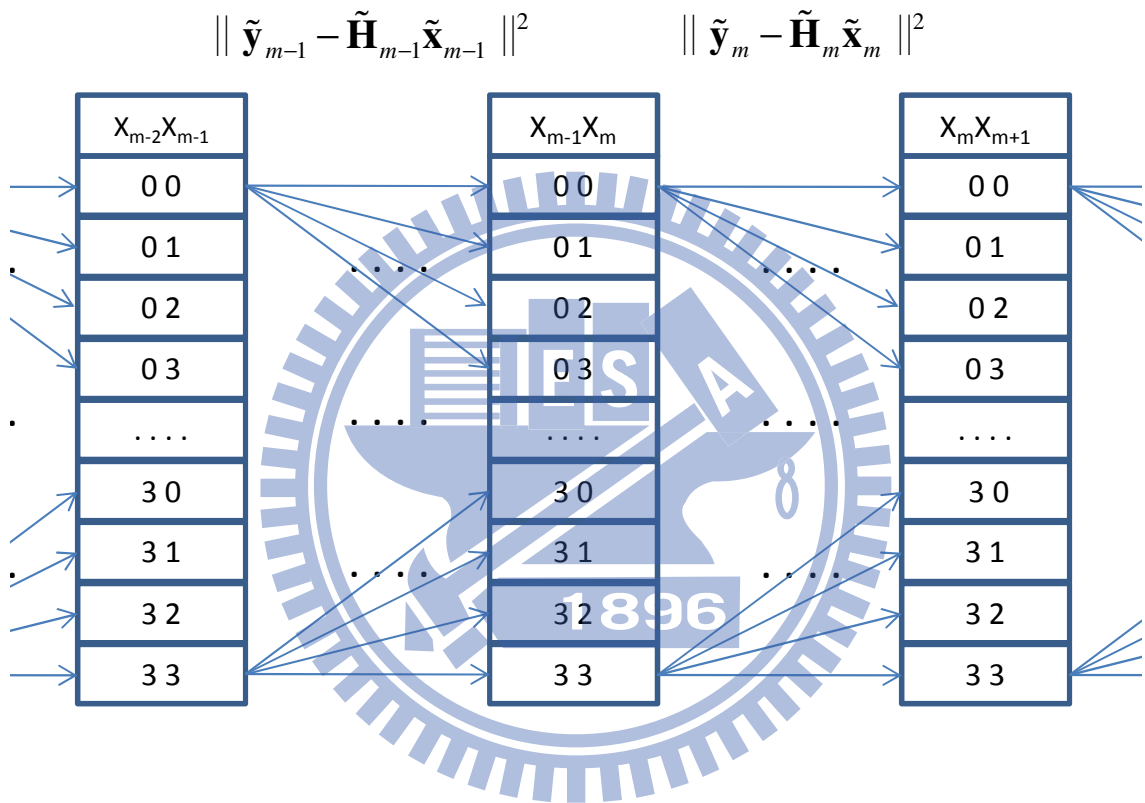


Figure 4.1: Trellis structure for MLSE-based detection using the Viterbi algorithm, under QPSK modulation and with $p = 1$, where numerals 0–3 represent the QPSK constellation points.

Table 4.1: Two Channel Power-Delay Profiles Used in This Study, Where TU6 Corresponds to the COST 207 6-Tap Typical Urban Channel And SUI4 the SUI-4 3-Tap Channel

TU6	Tap Index	1	2	3	4	5	6
	Delay (μs)	0.0	0.2	0.5	1.6	2.3	5.0
	Power (%)	19	38	24	9	6	4
SUI4	Tap Index	1	2	3	–	–	–
	Delay (μs)	0.0	1.5	4.0	–	–	–
	Power (%)	64	26	10	–	–	–

4.2 Complexity Analysis

Concerning complexity, let N_A denote the signal constellation size at each subcarrier. Then, for each subcarrier, the nonwhitening MLSE requires $O[(2K + 1)N_A^{2K+1}]$ complex multiplications and additions (CMAs) to build the trellis and $O(N_A^{2K+1})$ CMAs to conduct the Viterbi search [4]. In contrast, the proposed method requires $O[(2K + 1)N_A^{2p+1} + (2q + 1)^2 N_A^{2p+1}]$ CMAs to build the trellis, wherein $O[(2K + 1)N_A^{2p+1}]$ are for computing $\mathbf{H}_m \mathbf{x}_m$ and $O[(2q + 1)^2 N_A^{2p+1}]$ are for multiplying with $\mathbf{K}_z^{-\frac{1}{2}}$. Then the Viterbi search requires $O[(2q + 1)N_A^{2p+1}]$ CMAs. The computation of $\mathbf{K}_z^{-\frac{1}{2}}$ requires estimation of the ICI power and the AWGN power, but the complexity is far lower than building the trellis or performing the Viterbi search and is thus neglected. From the above, the proposed method may seem to require much higher complexity than nonwhitened MLSE. But, to the contrary, the reduced residual I+N through whitening may facilitate using a smaller ICI bandwidth K in the MLSE, culminating in a complexity gain rather than loss. This will be demonstrated in the simulation results below.

4.3 Simulation Results on Detection Performance

We present some simulation results on signal detection performance in this section. As in Sec. 3.2, we let subcarrier spacing $f_s = 10.94$ kHz and sample period $T_{sa} = 714$ ns. The subcarriers are QPSK-modulated with Gray-coded bit-to-symbol mapping. There is no channel coding. The channels are multipath Rayleigh-faded WSSUS channels having the PDPs shown in Table 4.1.

Unless otherwise noted, we let $N = 128$ and assume that the receiver has perfect knowledge of the channel state information (CSI), which includes the channel matrix within band K and the covariance matrix \mathbf{K}_z of the residual ICI plus noise.

To start, consider the extreme case of $K = 0$ in absence of channel noise. Through this we look at the limit imposed by the ICI to the performance of the conventional detection method. We also look at the possible gain from blockwise whitening of the full ICI followed by MLSE with $p = q = 1$, at infinite signal-to-noise ratio (SNR). The ICI covariance matrix in this case is given by

$$\mathbf{K}_z = \begin{bmatrix} 1 & 0.6 & 0.15 \\ 0.6 & 1 & 0.6 \\ 0.15 & 0.6 & 1 \end{bmatrix} \sigma_{c_0}^2 \quad (4.7)$$

where recall that $\sigma_{c_0}^2 = E[|c_{m,0}|^2]$ is the total ICI power. Fig. 4.2 shows some simulation results for the TU6 channel. The numerical performance for the SUI4 channel is very similar. These results show that ICI-whitening detection (the proposed technique) yields some advantage over conventional detection: the error probability is reduced by about 2.2 times.

Significantly higher gain can be obtained by ICI-whitening MLSE with $K = 1$. In Fig. 4.3 we compare the corresponding performance of the proposed technique with that of MLSE which treats the residual ICI as white [4], over TU6 and SUI4 channels in the noise-free condition (i.e., $\text{SNR} = \infty$). For the proposed technique, two parameter settings are considered, viz. $\{q = 1, p = 2\}$ and $\{q = 1, p = 1\}$, for

which the covariance matrices \mathbf{K}_z of residual ICI are given by, respectively,

$$\begin{bmatrix} 1 & 0.775 & 0.645 \\ 0.775 & 1 & 0.775 \\ 0.645 & 0.775 & 1 \end{bmatrix} \sigma_{c1}^2, \quad \begin{bmatrix} 1.785 & 1.16 & 1.16 \\ 1.16 & 1 & 1.16 \\ 1.16 & 1.16 & 1.785 \end{bmatrix} \sigma_{c1}^2, \quad (4.8)$$

where recall that $\sigma_{cK}^2 = E[|c_{m,K}|^2]$ is the residual ICI power outside band K .

Consider the case $p = q = 1$ first. In this case, the proposed method shows a remarkable gain of roughly three to four orders of magnitude in error performance compared to treating residual ICI as white. The error floor induced by the residual ICI can be driven to below 10^{-5} even at the very high normalized peak Doppler frequency of 0.32.

Very interestingly, Fig. 4.3 also shows that the setting $\{q = 1, p = 2\}$ yields a worse performance than $p = q = 1$, even though the former setting may seem more natural in its associated band channel matrix structure (compare (4.2) with (4.3)), which captures all the ICI terms within the modeling range ($K = 1$). Moreover, its corresponding trellis has more states than the latter setting (4^5 vs. 4^3). The reason will be explored in the next section. For now, we note that the above results appear to indicate the suitability of setting $p = q = K = 1$ in practical system design. It yields good performance without undue complexity. With this observation, we now present some more simulation results under this setting. The aims are to examine the proposed technique's performance at finite SNR and to compare it with a benchmarking upper bound. For this, we first consider how it varies with Doppler spread and then how it varies with SNR.

Fig. 4.4 shows some results for the TU6 channel with $p = q = K = 1$ at several SNR values. The results for SUI4 show similar characteristics and are omitted. We compare the performance of the proposed method with a benchmark: the matched-filter bound (MFB), i.e., signal detection with perfect knowledge of the interfering symbols. To make the MFB a more-or-less absolute lower bound, it is obtained with the residual ICI outside band K fully cancelled. Other than these, the same MLSE as in the proposed technique is used. For all three finite SNR values shown, note that the MFB drops monotonically with increasing f_d , i.e., with increasing time-variation

of the channel. This is in line with the fact that faster channel variation yields greater time diversity, as various researchers have observed [15,17,18]. However, such time diversity can show clearly only when ICI is sufficiently small (e.g., after ICI cancellation). For the proposed technique, its error performance at $E_b/N_0 = 15$ and 28 dB tracks that of the MFB reasonably closely, deviating by less than a multiplicative factor of three for normalized peak Doppler frequencies up to 0.18 ($f_d \leq 2000$ Hz). At $E_b/N_0 = 45$ dB, the performance improves with f_d until f_d reaches about 1500 Hz (normalized peak Doppler frequency ≈ 0.14). Afterwards, the residual ICI dominates in determining the performance, as can be seen by the closeness between the corresponding curves for $E_b/N_0 = 45$ dB and ∞ .

Next, consider how the performance of the proposed method varies with SNR. The solid lines in Fig. 4.5 show results at $f_d = 1500$ Hz (normalized peak Doppler frequency ≈ 0.14) under perfect CSI. It is seen that the proposed method at $K = 1$ can yield a substantial performance gain compared to nonwhitening MLSE [4] at $K = 2$. The dash-dot lines in Fig. 4.5 depict some results under imperfect CSI. Limited by space, we cannot elaborate on the many possible channel estimation methods and their performance. Hence the results shown pertain to a typical condition only. For this, we note that the mean-square channel estimation error is typically proportional to the variance of the unestimatable channel disturbance, with the proportionality constant inversely dependent on the sophistication of the channel estimation method [19]. In our case, the unestimatable channel disturbance includes residual ICI (mostly that beyond $K = 1$) and additive channel noise (AWGN). At a normalized peak Doppler frequency of 0.14 ($f_d = 1500$ Hz), the first term is approximately 20 dB below the received signal power. The proportionality constant is set to $1/8$. The channel estimation error limits the performance of all detection methods and the residual ICI-free bound in the form of error floors. The floor of the proposed method at $K = 1$ is seen to be lower than that of nonwhitening MLSE at $K = 2$ and is relatively close to the bound. We further note that, while Fig. 4.5 has been obtained with $N = 128$, the results obtained with $N = 1024$ (eight times the bandwidth) are very close.

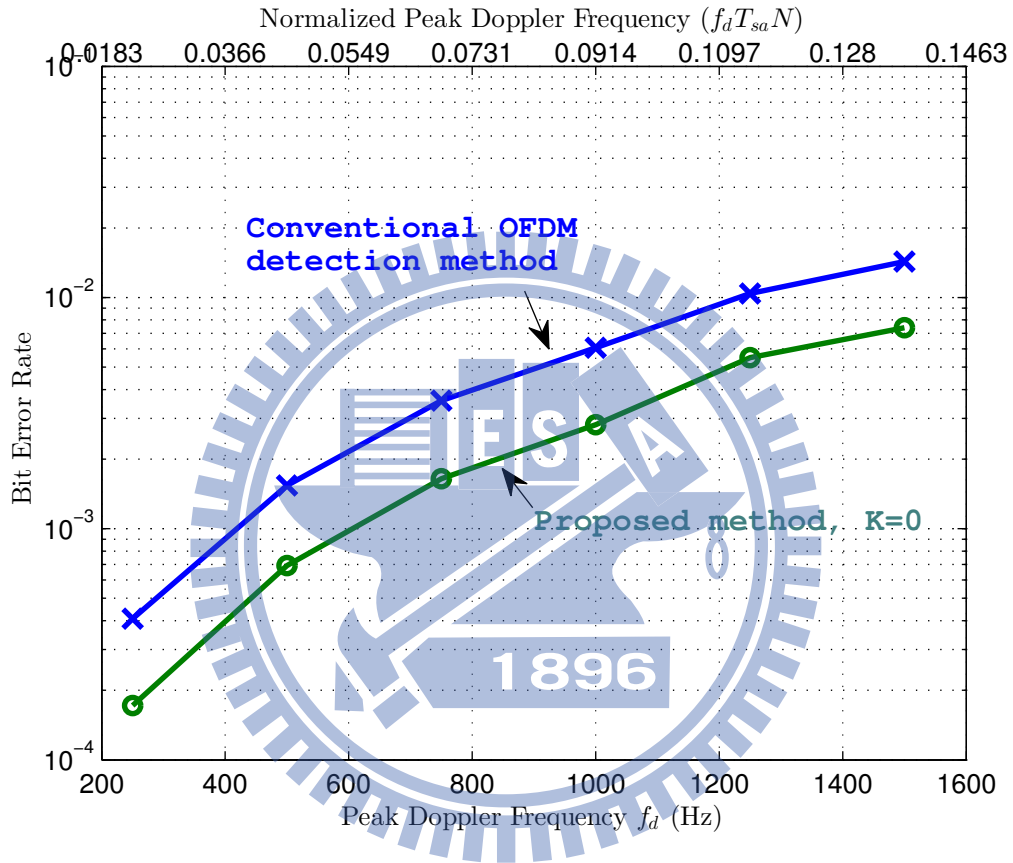


Figure 4.2: Error performance in TU6 channel of the conventional OFDM signal detection method and ICI-whitening MLSE (the proposed method) with $K = 0$ and $p = q = 1$ in noise-free condition.

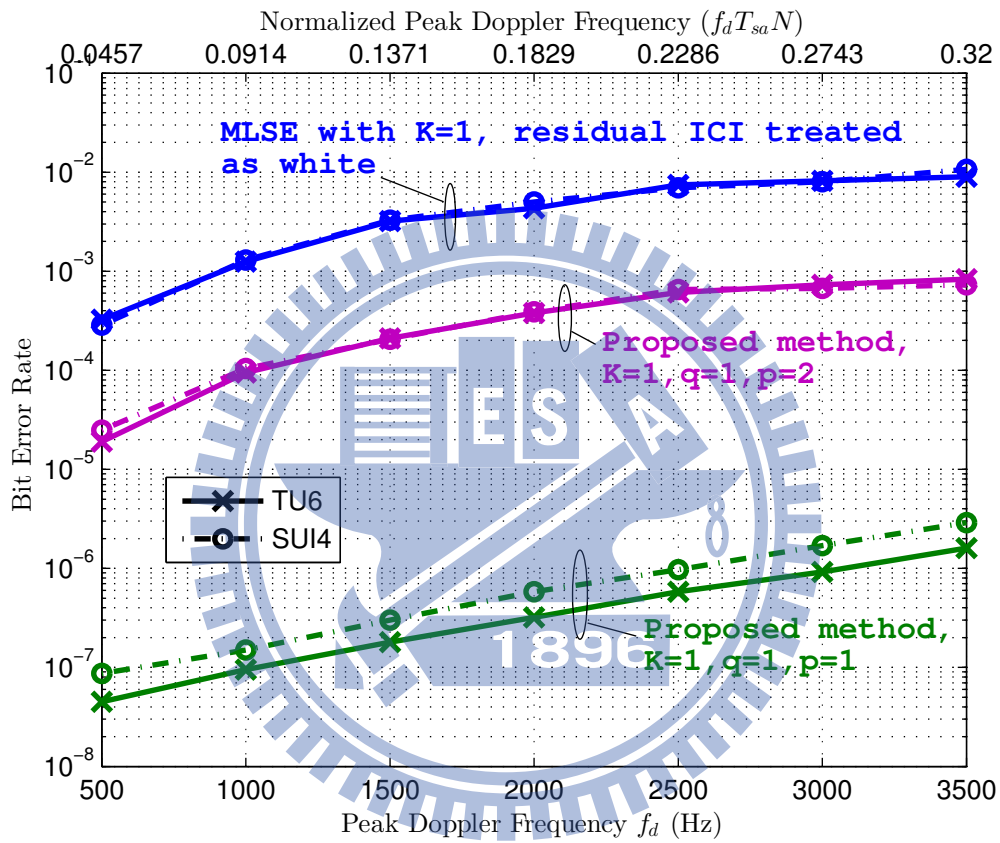


Figure 4.3: Comparison of proposed technique in TU6 and SUI4 channels with that treating residual ICI as white; $\text{SNR} = \infty$.

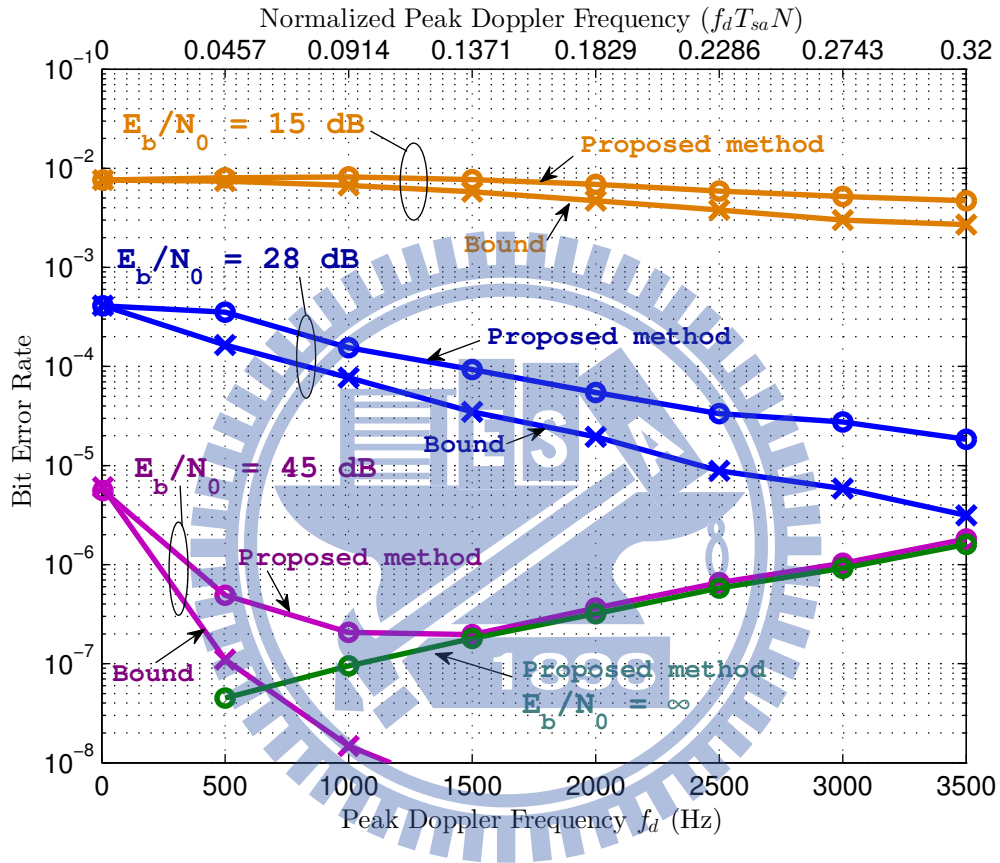


Figure 4.4: Performance of proposed technique versus Doppler spread in the TU6 channel with $p = q = K = 1$, at $N = 128$ and $T_{sa} = 714$ ns and under QPSK subcarrier modulation.

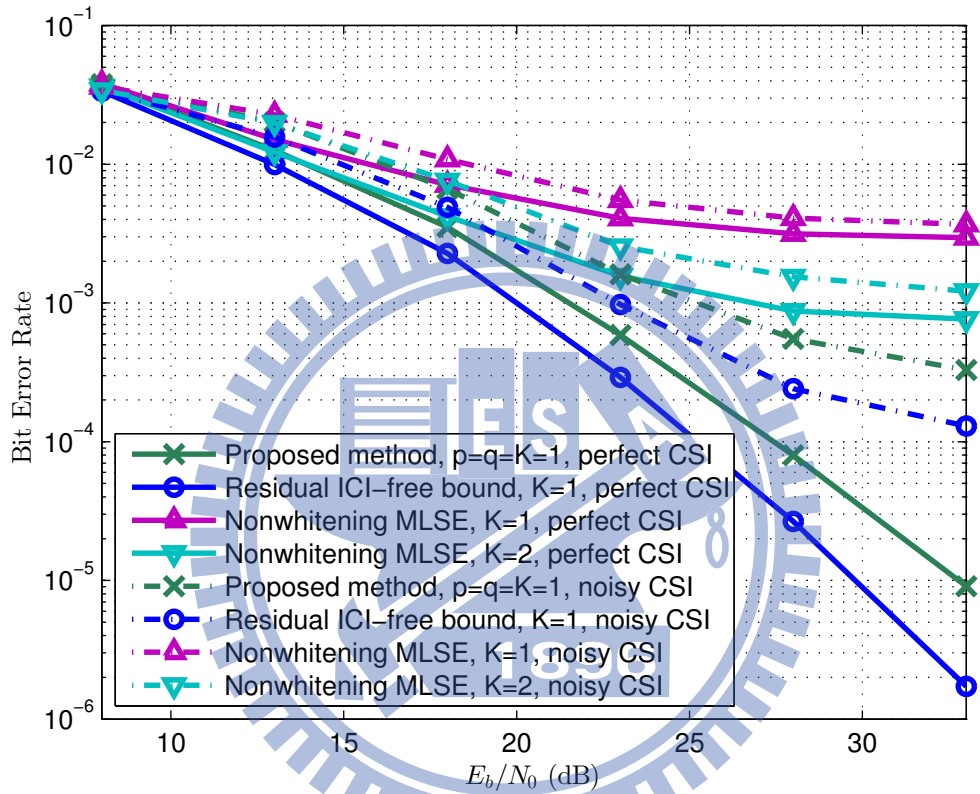


Figure 4.5: Performance versus E_b/N_0 of different methods in the TU6 channel, with $N = 128$, $T_{sa} = 714$ ns, $f_d = 1500$ Hz (normalized peak Doppler frequency $f_d T_{sa} N = 0.1371$) and QPSK subcarrier modulation. (Results with $N = 1024$ are very close.)

4.4 Dependence of Detection Performance on Parameter Setting

As mentioned, we here explore how signal detection performance depends on whitener parameter setting. In particular, recall that one intriguing phenomenon observed earlier is the worse performance with $p = 2$ than with $p = 1$ (both at $q = K = 1$), although the former is associated with a seemingly more natural-looking band channel matrix and a more expanded MLSE trellis. A comprehensive analysis would require examining the distance property of the received signal after the proposed blockwise whitening. However, a crude understanding can be obtained by looking at the signal-to-interference-plus-noise ratio (SINR) after blockwise whitening.

From (4.1) and (4.4), the pre- and post-whitening SINRs are given by, respectively,

$$\text{SINR}_{pre} = E[\mathbf{x}_m^H \mathbf{H}_m^H \mathbf{H}_m \mathbf{x}_m] / E[\mathbf{z}_m^H \mathbf{z}_m], \quad (4.9)$$

$$\text{SINR}_{post} = E[\mathbf{x}_m^H \mathbf{H}_m^H \mathbf{K}_z^{-1} \mathbf{H}_m \mathbf{x}_m] / E[\mathbf{z}_m^H \mathbf{K}_z^{-1} \mathbf{z}_m]. \quad (4.10)$$

For the power of residual ICI plus noise, we have $E[\mathbf{z}_m^H \mathbf{z}_m] = \text{tr}(E[\mathbf{z}_m \mathbf{z}_m^H]) = \text{tr}(\mathbf{K}_z)$ and $E[\mathbf{z}_m^H \mathbf{K}_z^{-1} \mathbf{z}_m] = \text{tr}(E[\mathbf{K}_z^{-1} \mathbf{z}_m \mathbf{z}_m^H]) = \text{tr}(\mathbf{K}_z^{-1} \mathbf{K}_z) = 2q + 1$, where $\text{tr}(\mathbf{A})$ denotes the trace of a matrix \mathbf{A} . For the signal power, we have $E[\mathbf{x}_m^H \mathbf{H}_m^H \mathbf{H}_m \mathbf{x}_m] = \text{tr}(E[\mathbf{H}_m^H \mathbf{H}_m \mathbf{x}_m \mathbf{x}_m^H]) = E_s \cdot \text{tr}(E[\mathbf{H}_m^H \mathbf{H}_m]) = E_s \cdot \text{tr}(E[\mathbf{H}_m \mathbf{H}_m^H])$ and $E[\mathbf{x}_m^H \mathbf{H}_m^H \mathbf{K}_z^{-1} \mathbf{H}_m \mathbf{x}_m] = \text{tr}(E[\mathbf{H}_m^H \mathbf{K}_z^{-1} \mathbf{H}_m \mathbf{x}_m \mathbf{x}_m^H]) = E_s \cdot \text{tr}(E[\mathbf{H}_m^H \mathbf{K}_z^{-1} \mathbf{H}_m]) = E_s \cdot \text{tr}(\mathbf{K}_z^{-1} E[\mathbf{H}_m \mathbf{H}_m^H])$, where E_s is as defined previously (the average energy of the transmitted signal samples) and we have assumed that the transmitted signal is independent and identically distributed (i.i.d.).

Note that the factor $E[\mathbf{H}_m \mathbf{H}_m^H]$ appears in the signal power terms of both SINRs. Employing a procedure similar to that for $E[c_{m,K} c_{m+r,K}^*]$ in Sec. 3.1, we can derive an expression for $E[\mathbf{H}_m \mathbf{H}_m^H]$ in terms of the channel parameters as in the case of $E[c_{m,K} c_{m+r,K}^*]$. However, although such an expression can provide more precise numerical results, an illuminating insight into the SNR impact of the proposed blockwise whitening technique can already be gathered with a very simple approx-

imation to $E[\mathbf{H}_m \mathbf{H}_m^H]$, and this insight is sufficient for the purpose of the present work. Specifically, in the limit of little ICI, \mathbf{H}_m approaches a diagonal matrix of the channel frequency response. In this case, $E[\mathbf{H}_m \mathbf{H}_m^H] \approx (\sum_{l=0}^{L-1} \sigma_l^2) \mathbf{I}$ where \mathbf{I} denotes an identity matrix and recall that we have assumed a unity channel power gain, i.e., $\sum_l \sigma_l^2 = 1$. Hence

$$\text{SINR}_{pre} \approx (2q + 1)E_s / \text{tr}(\mathbf{K}_z), \quad \text{SINR}_{post} \approx E_s \cdot \text{tr}(\mathbf{K}_z^{-1}) / (2q + 1). \quad (4.11)$$

As a result,

$$\frac{\text{SINR}_{post}}{\text{SINR}_{pre}} \approx \frac{\text{tr}(\mathbf{K}_z^{-1}) \cdot \text{tr}(\mathbf{K}_z)}{(2q + 1)^2}. \quad (4.12)$$

Now let λ_i , $0 \leq i \leq 2q$, denote the eigenvalues of \mathbf{K}_z . Then the eigenvalues of \mathbf{K}_z^{-1} are given by λ_i^{-1} and we have

$$\frac{\text{SINR}_{post}}{\text{SINR}_{pre}} \approx \frac{(\sum_{i=0}^{2q} \lambda_i^{-1}) (\sum_{i=0}^{2q} \lambda_i)}{(2q + 1)^2}. \quad (4.13)$$

Therefore, the more disparate the eigenvalues of \mathbf{K}_z are, the greater gain the proposed blockwise whitening can offer. If the eigenvalues are all equal, then no gain is attained.

As examples, we consider the previously considered cases 1) $\{K = 0, q = 1, p = 1\}$, 2) $\{K = 1, q = 1, p = 1\}$, and 3) $\{K = 1, q = 1, p = 2\}$, all at infinite SNR. The corresponding \mathbf{K}_z matrices are given in (4.7) and (4.8). For case 1), we obtain the eigenvalues $0.2232\sigma_{c0}^2$, $0.8500\sigma_{c0}^2$, and $1.9268\sigma_{c0}^2$; for case 2), $0.0654\sigma_{c1}^2$, $0.6250\sigma_{c1}^2$, and $3.8796\sigma_{c1}^2$; and for case 3), $0.1800\sigma_{c1}^2$, $0.3550\sigma_{c1}^2$, and $2.4650\sigma_{c1}^2$. The resulting post- to pre-SINR ratios are 2.0588, 8.7052, and 2.9258, respectively. They do correspond monotonically to the performance gains shown in Figs. 4.2 and 4.3. However, the mathematical relation between SINR and bit error rate (BER) is not straightforward—a point worth remembering when comparing the SINR performance of different detection methods and different parameter settings.

With the above caveat, we show some SINR performance results at finite SNR values in Fig. 4.6, both to verify the theory derived in this section and to further illustrate the performance of different detection methods. In the case of the proposed method, the theoretical SINR values shown in the figure have been obtained using (4.11), i.e., $\text{SINR}_{post} = E_s \cdot \text{tr}(\mathbf{K}_z^{-1}) / (2q + 1)$, whereas in the case of nonwhitening

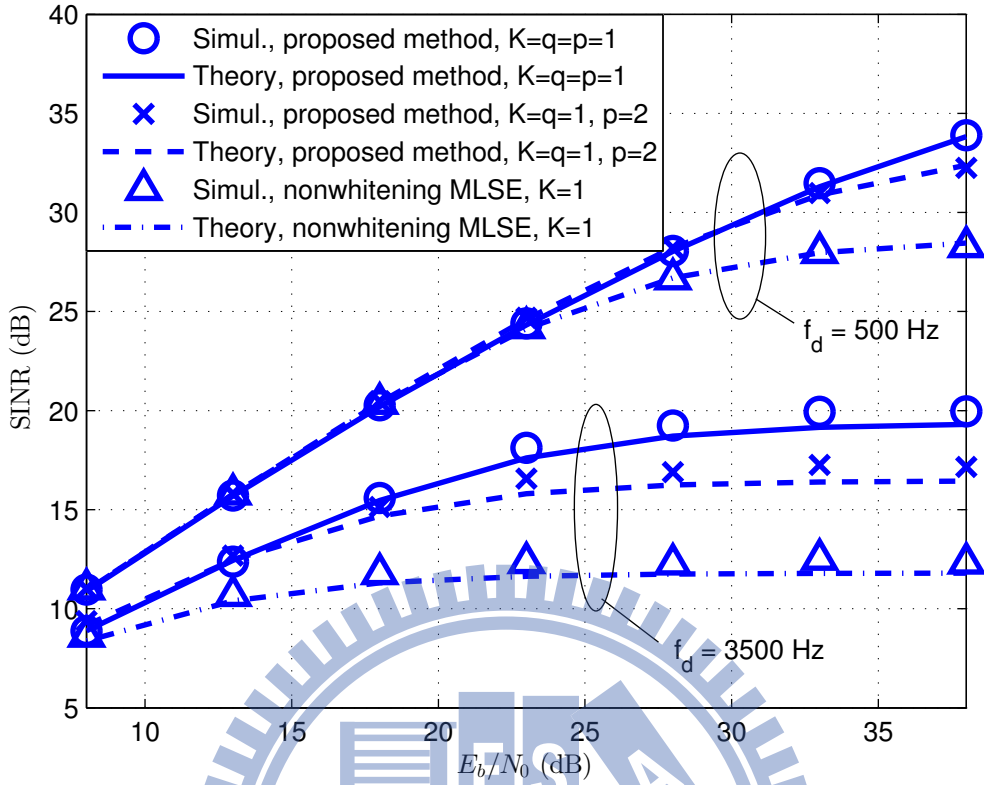


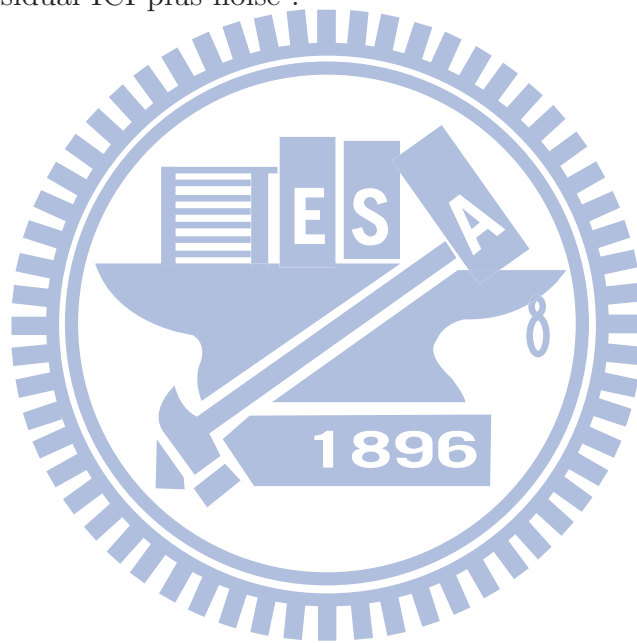
Figure 4.6: SINR performance of different methods in the TU6 channel, with $N = 128$ and $T_{sa} = 714$ ns and assuming perfect CSI.

MLSE, the values of “T” in the theoretical SINR are simply given by σ_{c1}^2 , which are calculated using (3.18) with $K = 1$. We see that, in the case $f_d = 500$ Hz (normalized peak Doppler frequency ≈ 0.046), the theory and the simulation results agree almost exactly, whereas in the case $f_d = 3500$ Hz (normalized peak Doppler frequency ≈ 0.32), the theory consistently underestimates the SINR performance by a fraction of a dB. The latter phenomenon can be understood by the fact that the σ_{c0}^2 as given in (3.17) is a progressively looser upper bound to the actual ICI power as the normalized peak Doppler frequency increases [11]. The figure confirms the earlier observation concerning the superiority of the proposed method with $K = q = p = 1$, especially in high SNR or high Doppler spread.

4.5 Summary of Results

We considered MLSE-type signal detection in ICI with blockwise whitening of the residual ICI plus noise. Simulations showed that the proposed technique could attain a substantially lower ICI-induced error floor than conventional MLSE.

To capitalize on the above high correlation to improve signal reception over fast varying channels, we consider performing simple blockwise whitening of the residual I+N before signal detection , where the whitener makes use of the ICI characteristics as found. SINR numerical results also show that substantial gains can be achieved with whitening residual ICI plus noise .



Chapter 5

Low Complexity Detection with Whitening of Residual ICI Plus Noise

The ICI is known to be colored [6,24]. Hence it is possible to reduce the error floor by whitening the residual “I+N” (i.e., sum of residual ICI and additive channel noise). But this would require knowing its autocorrelation function, which remained for a while an unsolved problem. Without knowing the autocorrelation function, one can only resort to less sophisticated techniques, such as simple differencing of the received signals at neighboring subcarriers [8]. Recently, we have obtained a characterization of the autocorrelation of the ICI [25]. It is shown that the normalized autocorrelation of the residual ICI is not only high, but also insensitive to a variety of system parameters and channel conditions including the sampling period T_{sa} , the DFT size N , the signal bandwidth, the average transmitted symbol energy E_s , the peak Doppler frequency f_d , and the channel power-delay profile (PDP). This is confirmed in [25] by simulation. As a result, the residual I+N can be whitened in a nearly channel-independent manner and, using MLSE as a demonstrator, we have shown that such whitening can facilitate significantly improved signal detection performance.

A main concern with MLSE is its complexity, especially with higher-order modulations. For reduced complexity, in this chapter we consider performing LMMSE and iterative LMMSE detection in association with the above mentioned whitening, together with soft decision feedback. Our LMMSE detector follows a similar principle as that proposed in [22,23], but contains modifications for improved performance. Simulations show that a good tradeoff between complexity and performance can be achieved.

In what follows, Sec. 5.1 presents the proposed detection method and Sec. 5.2 some simulation results. Finally, Sec. 5.3 gives the summary.

5.1 LMMSE Signal Detection with Whitening of Residual ICI Plus Noise

As indicated, in this chapter we consider LMMSE and iterative LMMSE signal detection, with partial whitening of additive disturbance (i.e., the residual I+N) to lower the error floor and with soft decision feedback.

Consider a vector of $2q+1$ frequency-domain signal samples centered at sample m , where q need not be equal to K :

$$\mathbf{y}_m = [Y_{m-q} \cdots Y_m \cdots Y_{m+q}]' = \mathbf{H}_m \mathbf{x}_m + \mathbf{z}_m \quad (5.1)$$

where $\mathbf{x}_m = [X_{m-p} \cdots X_m \cdots X_{m+p}]'$ for some integer p , \mathbf{H}_m is a $(2q+1) \times (2p+1)$ submatrix of channel matrix \mathbf{H} of bandwidth K , and \mathbf{z}_m collects all the right-hand-side (RHS) terms in (1.2) (or (1.4)) associated with Y_k , $m-q \leq k \leq m+q$, that do not appear in $\mathbf{H}_m \mathbf{x}_m$. The elements of \mathbf{z}_m include both residual ICI and channel noise. To avoid clogging the mathematical expressions, we have omitted explicit indexing of various quantities in (5.1) with the parameters K , p , and q , understanding that their dimensions and contents depend on these parameters. As

examples, with $\{K = 1, q = 1, p = 1\}$ we have

$$\mathbf{H}_m = \begin{bmatrix} a_{m-1,m-1} & a_{m-1,m} & 0 \\ a_{m,m-1} & a_{m,m} & a_{m,m+1} \\ 0 & a_{m+1,m} & a_{m+1,m+1} \end{bmatrix} \quad (5.2)$$

and with $\{K = 2, q = 1, p = 1\}$,

$$\mathbf{H}_m = \begin{bmatrix} a_{m-1,m-1} & a_{m-1,m} & a_{m-1,m+1} \\ a_{m,m-1} & a_{m,m} & a_{m,m+1} \\ a_{m+1,m-1} & a_{m+1,m} & a_{m+1,m+1} \end{bmatrix}. \quad (5.3)$$

A tradeoff between complexity and performance can be achieved by judicious choice of $\{K, q, p\}$.

Let $\mathbf{K}_{\mathbf{u}\mathbf{v}}$ denote the covariance matrix of random vectors \mathbf{u} and \mathbf{v} , i.e., $\mathbf{K}_{\mathbf{u}\mathbf{v}} = E[(\mathbf{u} - E\{\mathbf{u}\})(\mathbf{v} - E\{\mathbf{v}\})^H]$ where superscript H denotes Hermitian transpose. When $\mathbf{u} = \mathbf{v}$, we simply write $\mathbf{K}_{\mathbf{u}}$. For simplicity, rather than performing whitening over a complete sequence, we do blockwise whitening of the residual I+N over windows of size $2q + 1$ as

$$\tilde{\mathbf{y}}_m \triangleq \mathbf{K}_{\mathbf{z}}^{-\frac{1}{2}} \mathbf{y}_m = \underbrace{\mathbf{K}_{\mathbf{z}}^{-\frac{1}{2}} \mathbf{H}_m}_{\triangleq \tilde{\mathbf{H}}_m} \mathbf{x}_m + \underbrace{\mathbf{K}_{\mathbf{z}}^{-\frac{1}{2}} \mathbf{z}_m}_{\triangleq \tilde{\mathbf{z}}_m} \quad (5.4)$$

where we have omitted the subscript m in $\mathbf{K}_{\mathbf{z}}$ due to its invariance over m . The quantity $\mathbf{K}_{\mathbf{z}}^{-\frac{1}{2}}$ may be defined in more than one way; for example, we may let $\mathbf{K}_{\mathbf{z}}^{-\frac{1}{2}} = \mathbf{U}\mathbf{\Lambda}^{-\frac{1}{2}}\mathbf{U}^H$ where \mathbf{U} is the matrix of orthonormal eigenvectors of $\mathbf{K}_{\mathbf{z}}$ and $\mathbf{\Lambda}$ is the diagonal matrix of corresponding eigenvalues of $\mathbf{K}_{\mathbf{z}}$.

If we treat each signal block (window) separately without regard to their partially overlapping relationship, then the LMMSE estimate of some X_d in \mathbf{x}_m (where $m - p \leq d \leq m + p$), conditioned on prior estimates of all other elements of \mathbf{x}_m , is given by [22,26]

$$\begin{aligned} \hat{X}_d^{(m)} &= \mathbf{K}_{\tilde{\mathbf{y}}_m X_d | \bar{\mathbf{x}}_m}^H \mathbf{K}_{\tilde{\mathbf{y}}_m | \bar{\mathbf{x}}_m}^{-1} (\tilde{\mathbf{y}}_m - E[\tilde{\mathbf{y}}_m | \bar{\mathbf{x}}_m^{(d)}]) \\ &= \mathbf{K}_{\tilde{\mathbf{y}}_m X_d | \bar{\mathbf{x}}_m}^H \mathbf{K}_{\tilde{\mathbf{y}}_m | \bar{\mathbf{x}}_m}^{-1} (\tilde{\mathbf{y}}_m - \tilde{\mathbf{H}}_m \bar{\mathbf{x}}_m^{(d)}) \end{aligned} \quad (5.5)$$

where $\bar{\mathbf{x}}_m^{(d)} = [\bar{X}_{m-p}, \dots, \bar{X}_{d-1}, 0, \bar{X}_{d+1}, \dots, \bar{X}_{m+p}]'$ is a vector of prior estimates of X_k , $k = m - p, \dots, d - 1, d + 1, \dots, m + p$ (with overbars indicating their being prior

estimates) and the notation “ $|\bar{\mathbf{x}}_m^{(d)}$ ” indicates conditioning on $\bar{\mathbf{x}}_m^{(d)}$. The term $\tilde{\mathbf{H}}_m \bar{\mathbf{x}}_m^{(d)}$ gives the contribution of the priors (except that at subcarrier d) in the received signal $\tilde{\mathbf{y}}_m$. With X_k assumed white, we have $\mathbf{K}_{\tilde{\mathbf{y}}_m X_d | \bar{\mathbf{x}}_m^{(d)}} = E_s \tilde{\mathbf{h}}_m^{(d)}$, where $\tilde{\mathbf{h}}_m^{(d)}$ stands for the $(d-m+p+1)$ th column of $\tilde{\mathbf{H}}_m$. Further, we have $\mathbf{K}_{\tilde{\mathbf{y}}_m | \bar{\mathbf{x}}_m^{(d)}} = \tilde{\mathbf{H}}_m \mathbf{K}_{\mathbf{x}_m | \bar{\mathbf{x}}_m^{(d)}} \tilde{\mathbf{H}}_m^H + \mathbf{I}$ where $\mathbf{K}_{\mathbf{x}_m | \bar{\mathbf{x}}_m^{(d)}} = E[(\mathbf{x}_m - \bar{\mathbf{x}}_m^{(d)})(\mathbf{x}_m - \bar{\mathbf{x}}_m^{(d)})^H | \bar{\mathbf{x}}_m^{(d)}]$. It has been observed, albeit in different contexts than the present work, that ignoring the nondiagonal terms of $\mathbf{K}_{\mathbf{x}_m | \bar{\mathbf{x}}_m^{(d)}}$ only results in minor performance loss [27,28]. Previous works on iterative LMMSE ICI equalization have also adopted a diagonal approximation to the conditional signal covariance matrix [22,23]. Therefore, we also employ such a diagonal approximation for simplicity: $\mathbf{K}_{\mathbf{x}_m | \bar{\mathbf{x}}_m^{(d)}} \approx \mathbf{V}_m^{(d)} \approx \text{diag}(v_{m-p}, \dots, v_{d-1}, E_s, v_{d+1}, \dots, v_{m+p})$ where $v_k = E[|X_k|^2 | \bar{X}_k] - |\bar{X}_k|^2$, $k = m-p, \dots, d-1, d+1, \dots, m+p$. Carrying out the above estimation for each X_d in each \mathbf{x}_m would yield $2p+1$ estimates for each signal sample.

Based on the above, our LMMSE detector considers each X_d in each \mathbf{x}_m in sequence and conducts conditional LMMSE estimation as described, with the needed priors formed by soft-combining the most recent $2p+1$ estimates of X_k , $k \neq d$. After completing the estimation of all X_d in all \mathbf{x}_m , the process may be repeated over the same signal samples, resulting in iterative LMMSE detection. The above procedure resembles the “sequential iterative estimation (SIE)” method of [22] except for multiple (i.e., $2p+1$) estimations of each signal sample and their soft combination. Simulation results show that these modifications can yield significant performance gain. We now explain the method of soft combination.

First, we set up a buffer of $(2p+1)N$ entries to hold $\hat{X}_d^{(m)} \forall d \forall m$. The buffer entries are initialized to zero. A new estimate $\hat{X}_d^{(m)}$ immediately overwrites the previous value recorded in the corresponding entry and is used in subsequent soft combination. In soft-combining the multiple estimates, we take the average of signal values over the posterior probability distribution as

$$\bar{X}_d = \sum_{\xi \in \Xi} \xi P(X_d = \xi | \hat{\mathbf{x}}_d) = \frac{\sum_{\xi \in \Xi} \xi f(\hat{\mathbf{x}}_d | X_d = \xi)}{\sum_{\xi \in \Xi} f(\hat{\mathbf{x}}_d | X_d = \xi)} \quad (5.6)$$

where Ξ denotes the signal constellation, $\hat{\mathbf{x}}_d = [\hat{X}_d^{(d-p)}, \dots, \hat{X}_d^{(d+p)}]'$, $P(X_d = \xi | \hat{\mathbf{x}}_d)$ denotes the posterior probability of $X_d = \xi$, and $f(\hat{\mathbf{x}}_d | X_d = \xi)$ denotes the likelihood

function of $\hat{\mathbf{x}}_d$ for $X_d = \xi$. For simplicity, assume that the likelihood function observes a jointly circularly Gaussian distribution as

$$f(\hat{\mathbf{x}}_d|X_d = \xi) = \frac{1}{c} e^{-\frac{1}{2}(\hat{\mathbf{x}}_d - \mathbf{u}_\xi)^H \mathbf{K}_\xi^{-1} (\hat{\mathbf{x}}_d - \mathbf{u}_\xi)} \quad (5.7)$$

where c is an inconsequential constant, $\mathbf{u}_\xi = E[\hat{\mathbf{x}}_d|X_d = \xi]$, and \mathbf{K}_ξ denotes the covariance matrix of $\hat{\mathbf{x}}_d$ conditioned on $X_d = \xi$.

To avoid the complexity of working with a full \mathbf{K}_ξ matrix, we approximate it by $\frac{1}{s} \hat{\mathbf{K}}_\xi$ where $\hat{\mathbf{K}}_\xi$ is a diagonal matrix that has the same diagonal elements as \mathbf{K}_ξ and s is a subunity factor to compensate for the (statistically) over-optimistic likelihood characterization arising from omission of the nondiagonal terms in \mathbf{K}_ξ . This is similar to what has been considered in turbo decoding [29,30], and a factor $s = 0.7$ is suggested in [30] based on simulation. We also let $s = 0.7$ in our simulation. Concerning the elements of \mathbf{u}_ξ and $\hat{\mathbf{K}}_\xi$, we have

$$E[\hat{X}_d^{(m)}|X_d = \xi] = \mathbf{g}_m^{(d)H} \tilde{\mathbf{h}}_m^{(d)} \xi \quad (5.8)$$

and

$$\hat{\mathbf{K}}_\xi = \frac{1}{2} \text{diag}([\sigma_d^{(d-p)}(\xi)]^2, \dots, [\sigma_d^{(d+p)}(\xi)]^2) \quad (5.9)$$

with

$$[\sigma_d^{(m)}(\xi)]^2 = \mathbf{g}_m^{(d)H} \tilde{\mathbf{h}}_m^{(d)} (1 - \tilde{\mathbf{h}}_m^{(d)H} \mathbf{g}_m^{(d)}), \quad (5.10)$$

where $d-p \leq m \leq d+p$ and $\mathbf{g}_m^{(d)} \triangleq (\tilde{\mathbf{H}}_m \mathbf{V}_m^{(d)} \tilde{\mathbf{H}}_m^H + \mathbf{I})^{-1} \tilde{\mathbf{h}}_m^{(d)}$. Also for simplicity, for QAM the update (5.6) is carried out in the I and Q directions separately, which is particularly appropriate under Gray coding.

5.2 Simulation Results

Consider an OFDM system with DFT size $N = 128$, subcarrier spacing $f_s = 10.94$ kHz, and sample period $T_{sa} = 1/(Nf_s) = 714$ ns, which are some of the Mobile WiMAX parameters. Let there be no channel coding. The modulations employ Gray-coded bit-to-symbol mapping. The channel is WSSUS with PDP as shown in Table 4.1 and with each path subject to Rayleigh fading. Assume that the

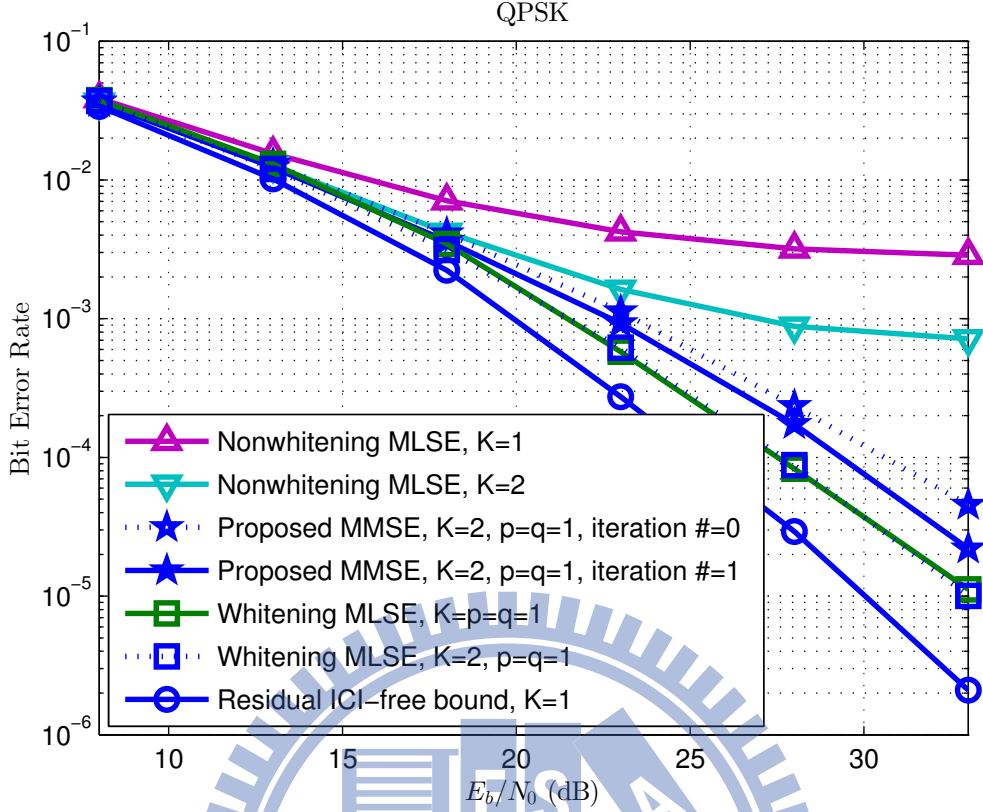


Figure 5.1: Bit error rate of different detection methods in the TU6 channel, with $N = 128$, $T_{sa} = 714$ ns, $f_d = 1500$ Hz (normalized peak Doppler frequency $f_d T_{sa} N = 0.1371$) and QPSK subcarrier modulation.

receiver has perfect channel state information (CSI), which includes the channel matrix within band K and the covariance matrix \mathbf{K}_z of the residual I+N.

First, consider QPSK subcarrier modulation in a relatively high $f_d = 1500$ Hz (normalized peak Doppler frequency ≈ 0.14). Let $\{K = 2, p = q = 1\}$. From the theory outlined in Sec. III, it can be derived that the normalized autocorrelation matrix of the out-of-band (i.e., residual) ICI is given by

$$\begin{bmatrix} 1.62 & 1.17 & 1.17 \\ 1.17 & 1 & 1.17 \\ 1.17 & 1.17 & 1.62 \end{bmatrix}. \quad (5.11)$$

The first four curves in Fig. 5.1 compare the performance of the proposed technique with that of MLSE which treats the residual ICI as white [4]. They show that the proposed method can yield a substantial gain compared to nonwhitening MLSE at

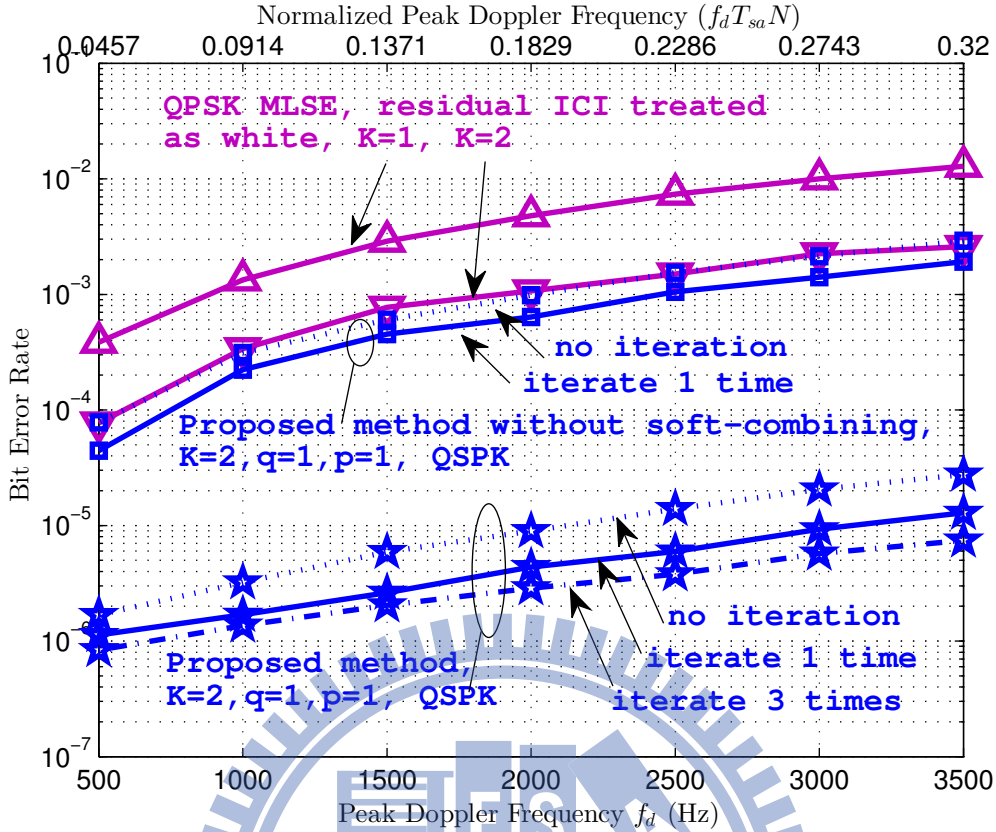


Figure 5.2: Bit error rate floor versus Doppler spread of different detection methods in the TU6 channel with $N = 128$, $T_{sa} = 714$ ns, and QPSK subcarrier modulation.

both $K = 1$ and $K = 2$. For additional comparison, we also show the performance of the whitened MLSE of [25] and a benchmark, namely, the matched-filter bound (MFB). The MFB does MLSE with perfect knowledge of the interfering symbols and with the residual ICI outside band K fully cancelled. Not surprisingly, the whitened MLSE has a better performance, but the proposed LMMSE technique has a much lower complexity and thus provides a good complexity-performance tradeoff.

We now examine the ICI-induced error floors of different techniques. Fig. 5.2 shows the results of the proposed technique (with soft-combined feedback) and that of MLSE which treats the residual ICI as white [4], over a large range of peak Doppler frequencies under QPSK subcarrier modulation. For the proposed technique, we again let $\{K = 2, p = q = 1\}$. The proposed method (three bottom curves) shows a remarkable gain of roughly two to three orders of magnitude compared to treating the residual ICI as white (two top curves). The error floor can be

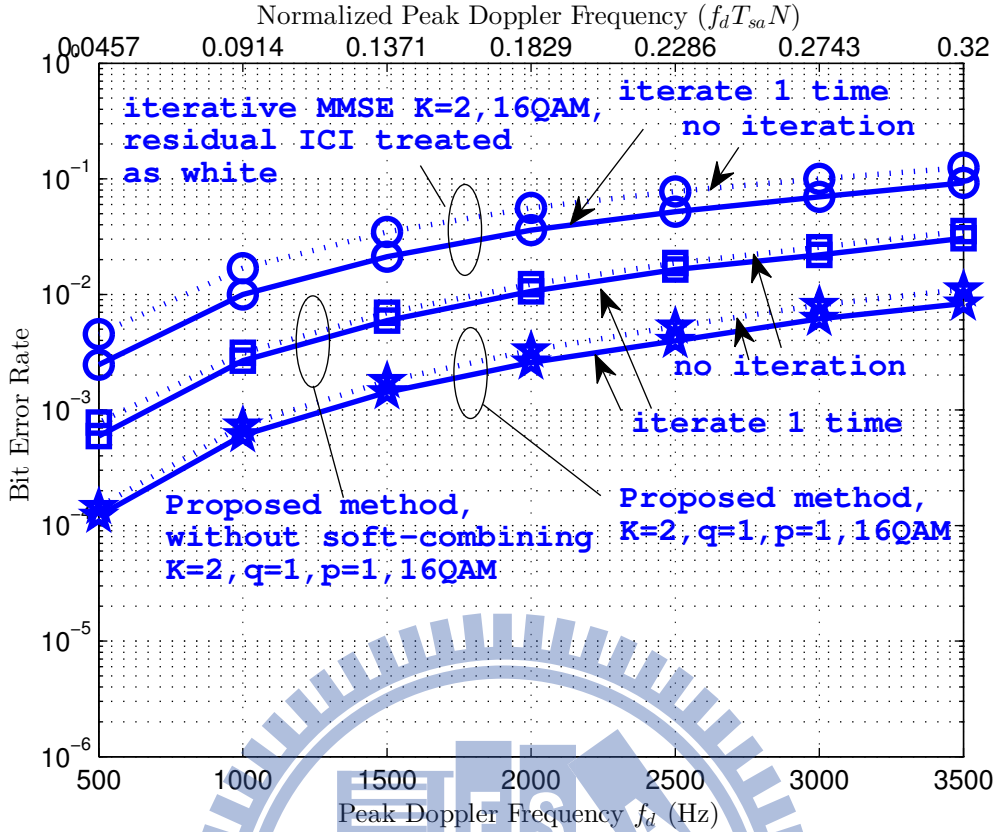


Figure 5.3: Bit error rate floor versus Doppler spread of different detection methods in the TU6 channel with $N = 128$, $T_{sa} = 714$ ns, and 16QAM subcarrier modulation.

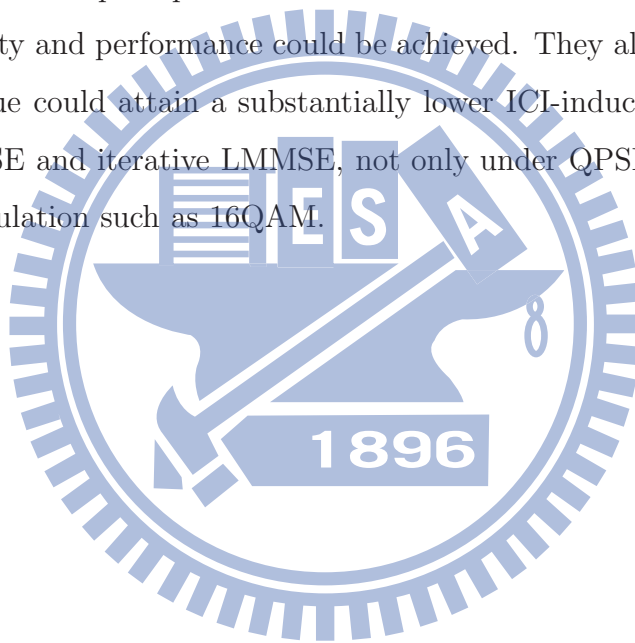
driven to well below 10^{-4} even at the very high normalized peak Doppler frequency of 0.32. The results also shows that, under the simulated conditions, one iteration of the proposed method may already provide close to what more iterations can provide in performance. For comparison, we also show the performance of LMMSE without soft combination in feedback, i.e., with $\bar{X}_k = \hat{X}_k^{(k)} \forall k$ (two middle curves). There is obvious gain from performing soft combination.

In Fig. 5.3, we look at the ICI-induced error floors of different methods under 16QAM subcarrier modulation. As MLSE-based techniques appear too complicated with high-order modulations, we only consider LMMSE methods. We compare the performance of the proposed method with the sequential iterative LMMSE (without whitening of residual I+N) of [22]. In the proposed method, we again let $\{K = 2, p = q = 1\}$. We see that there is still an order-of-magnitude performance gain with the proposed technique under 16QAM, with soft-combined feedback. This can be highly

beneficial when coupled with channel coding.


5.3 Summary of Results

In this chapter, we considered LMMSE signal detection with blockwise whitening of residual ICI plus noise. After whitening, the method performed conditional LMMSE equalization of each signal sample in a sequential manner, enlisting previously equalized samples at nearby subcarriers in soft-combined feedback to enhance detection performance. We presented some simulation results based on 3×3 block whitening and three-sample equalization. The results showed that a good tradeoff between complexity and performance could be achieved. They also showed that the proposed technique could attain a substantially lower ICI-induced error floor than conventional MLSE and iterative LMMSE, not only under QPSK but also under a higher-order modulation such as 16QAM.



Chapter 6

Thesis Conclusions and Potential Future Topics



In time-varying channels, OFDM transmission suffers from ICI. In a system without ICI, the channel frequency response matrix that relates the inputs of the inverse discrete Fourier transform (IDFT) and the outputs of the DFT is diagonal. Fast channel variation introduces sizable off-diagonal elements in the matrix, thus resulting in ICI. As stated previously, a band approximation to channel matrix that retains only the dominant terms about the diagonal may ease receiver design, but also results in an irreducible noise floor at receiver.

In this thesis, we exploit the correlation of the residual ICI outside the band of channel matrix to attain a significantly enhanced signal detection performance.

6.1 Thesis Conclusions

In Chap. 3, we found that, in a mobile time-varying channel, the residual ICI beyond several dominant terms had high normalized autocorrelation. We derived a rather precise closed-form approximation for the (unnormalized) autocorrelation function. It turns out that, up to a rather high peak Doppler frequency, the normalized

autocorrelation was not sensitive to a variety of system parameters and channel conditions, including the DFT size, the sample period, the system bandwidth, the OFDM symbol period, the average transmitted symbol energy, the multipath channel profile, and the Doppler PSDs of the channel paths. As a result, a whitening transform for the residual ICI plus noise can be obtained based solely on the ICI-to-noise ratio. A whitening transform depends on the ICI-to-noise ratio but no other quantities also implies that it is easy to be estimated.

Such a whitening transform can be used in association with many different detection schemes and significantly improves the performance.

In Sec. 4.1, we considered MLSE-type signal detection with blockwise whitening of the residual ICI plus noise. Simulations showed that the proposed technique could lower the ICI induced error floor by several orders of magnitude in MLSE that addressed a few dominant ICI terms.

To capitalize on the above high correlation to improve signal reception over fast varying channels, in Sec. 4.4, we consider performing simple blockwise whitening of the residual I+N before signal detection (i.e., equalization), where the whitener makes use of the ICI characteristics as found. Numerical analysis of SINR also confirms that substantial gains can be achieved with this approach.

In Chap. 5 , we considered LMMSE signal detection with blockwise whitening of residual ICI plus noise. After whitening, the method performed conditional LMMSE equalization of each signal sample in a sequential manner, enlisting previously equalized samples at nearby subcarriers in soft-combined feedback to enhance detection performance. We presented some simulation results based on 3×3 block whitening and three-sample equalization. They showed that a good tradeoff between complexity and performance could be achieved.

6.2 Potential Future Research Topics

- As mention above, we explore the correlation property of ICI outside the band and derive an approximate mathematical expression from it. We found that the correlation values are based solely on the ICI-to-noise ratio. It should be noted that the ICI correlation property derived applies not only to the flat fading, but also to the frequency selective fading. Furthermore, this property applies not only to classical multipath Rayleigh fading, but also to arbitrary different Doppler spectrum shapes in each path. The assumptions of approximate expression of normalized ICI autocorrelation are so general that we can extend ICI correlation property to many applications. Even for different frequency offsets or Doppler spectrums coming from multiple transmitters and channels, this approximation of normalized ICI autocorrelation still works. Some interesting topics arise and worth investigating:

- ICI and CFO mitigation in MIMO OFDM
- ICI and CFO mitigation in Cooperative OFDM
- ICI and CFO mitigation in OFDMA

- Through this assumption of perfect channel knowledge, the improvement of the detection performance confirms the substantial gains of numerical analysis in Sec. 4.1. On the other hand, we keep digging into most of our research based on the assumption of perfect channel knowledge until now. More detail of the actual implementation of ICI correlation property should be go through.

- We should incorporate the online estimation of covariance matrix of residual ICI plus noise into the proposed detection.
- We may incorporate channel estimation into the proposed LMMSE detection, which may resolve the estimation error of CSI.
- We may also incorporate the FEC decoder into the proposed LMMSE detection with blockwise whitening of residual ICI plus noise. This scheme is a form of turbo equalization.

Appendix A: The Whiteners of Residual ICI Plus Noise

As mentioned in Chap. 4 and 5, we do blockwise whitening over windows of size $2q+1$ by \mathbf{K}_z , which depends on the settings of q, p, K . In this Appendix, we consider all \mathbf{K}_z listed in the thesis and illustrate how these whitener are calculated from the properties of autocorrelation of residual ICI in Chap. 3.

As defined in Chap. 4, we have $\mathbf{K}_z = E[\mathbf{z}_m \mathbf{z}_m^H]$ and the aforesaid blockwise whitening of residual ICI plus noise \mathbf{z}_m is given by

$$\tilde{\mathbf{y}}_m \triangleq \mathbf{K}_z^{-\frac{1}{2}} \mathbf{y}_m = \underbrace{\mathbf{K}_z^{-\frac{1}{2}} \mathbf{H}_m}_{\triangleq \tilde{\mathbf{H}}_m} \mathbf{x}_m + \underbrace{\mathbf{K}_z^{-\frac{1}{2}} \mathbf{z}_m}_{\triangleq \tilde{\mathbf{z}}_m}$$

A tradeoff between complexity and performance can be achieved by choosing q, p , and K . All the settings of $\{q, p, K\}$ that have been used in the thesis are as follows:

- $\{K = 1, q = 1, p = 2\}$,

$$\mathbf{H}_m = \begin{bmatrix} a_{m-1,m-2} & a_{m-1,m-1} & a_{m-1,m} & 0 & 0 \\ 0 & a_{m,m-1} & a_{m,m} & a_{m,m+1} & 0 \\ 0 & 0 & a_{m+1,m} & a_{m+1,m+1} & a_{m+1,m+2} \end{bmatrix} \quad (\text{A.1})$$

- $\{K = 0, q = 1, p = 1\}$,

$$\mathbf{H}_m = \begin{bmatrix} a_{m-1,m-1} & 0 & 0 \\ 0 & a_{m,m} & 0 \\ 0 & 0 & a_{m+1,m+1} \end{bmatrix} \quad (\text{A.2})$$

- $\{K = 1, q = 1, p = 1\}$,

$$\mathbf{H}_m = \begin{bmatrix} a_{m-1,m-1} & a_{m-1,m} & 0 \\ a_{m,m-1} & a_{m,m} & a_{m,m+1} \\ 0 & a_{m+1,m} & a_{m+1,m+1} \end{bmatrix}. \quad (\text{A.3})$$

- $\{K = 2, q = 1, p = 1\}$,

$$\mathbf{H}_m = \begin{bmatrix} a_{m-1,m-1} & a_{m-1,m} & a_{m-1,m+1} \\ a_{m,m-1} & a_{m,m} & a_{m,m+1} \\ a_{m+1,m-1} & a_{m+1,m} & a_{m+1,m+1} \end{bmatrix}. \quad (\text{A.4})$$

Values of the Whiteners of Residual ICI (Infinite SNR)

At infinite SNR, consider the setting $\{K = 1, q = 1, p = 2\}$ as (A.1), for which the covariance matrices \mathbf{K}_z of residual ICI ($Z_m = c_{m,k}$) is given by

$$\mathbf{K}_z|_{\{K=1,q=1,p=2\}} = \begin{bmatrix} E[|c_{m,1}|^2] & E[c_{m,1}c_{m+1,1}^*] & E[c_{m,1}c_{m+2,1}^*] \\ E[c_{m,1}c_{m+1,1}^*]^* & E[|c_{m,1}|^2] & E[c_{m,1}c_{m+1,1}^*] \\ E[c_{m,1}c_{m+2,1}^*]^* & E[c_{m,1}c_{m+1,1}^*]^* & E[|c_{m,1}|^2] \end{bmatrix} \quad (\text{A.5})$$

By Fig. 3.1 or (3.8), we get

$$\mathbf{K}_z|_{\{K=1,q=1,p=2\}} = \begin{bmatrix} 1 & 0.775 & 0.645 \\ 0.775 & 1 & 0.775 \\ 0.645 & 0.775 & 1 \end{bmatrix} \sigma_{c1}^2. \quad (\text{A.6})$$

where $\sigma_{c1}^2 = E[|c_{m,1}|^2]$ is the residual ICI power outside band $K=1$.

Similarly,

$$\mathbf{K}_z|_{\{K=0,q=1,p=1\}} = \begin{bmatrix} E[|c_{m,0}|^2] & E[c_{m,0}c_{m+1,0}^*] & E[c_{m,0}c_{m+2,0}^*] \\ E[c_{m,0}c_{m+1,0}^*]^* & E[|c_{m,0}|^2] & E[c_{m,0}c_{m+1,0}^*] \\ E[c_{m,0}c_{m+2,0}^*]^* & E[c_{m,0}c_{m+1,0}^*]^* & E[|c_{m,0}|^2] \end{bmatrix} \quad (\text{A.7})$$

$$= \begin{bmatrix} 1 & 0.6 & 0.15 \\ 0.6 & 1 & 0.6 \\ 0.15 & 0.6 & 1 \end{bmatrix} \sigma_{c0}^2. \quad (\text{A.8})$$

where $\sigma_{c_0}^2 = E[|c_{m,0}|^2]$ is the residual ICI power outside band $K=0$.

Next, we consider the setting $\{K = 1, q = 1, p = 1\}$ as (A.3). By comparing \mathbf{H}_m in (A.3) with (A.1), we note that the absent items $a_{m-1,m-2}$ and $a_{m+1,m+2}$, which should be considered by rearranging the terms of sum in (3.5) or (3.14).

$$\mathbf{K}_z|_{\{K=1,q=1,p=1\}} = \begin{bmatrix} 1.785 & 1.16 & 1.16 \\ 1.16 & 1 & 1.16 \\ 1.16 & 1.16 & 1.785 \end{bmatrix} \sigma_{c_1}^2. \quad (\text{A.9})$$

Similarly,

$$\mathbf{K}_z|_{\{K=2,q=1,p=1\}} = \begin{bmatrix} 1.62 & 1.17 & 1.17 \\ 1.17 & 1 & 1.17 \\ 1.17 & 1.17 & 1.62 \end{bmatrix} \sigma_{c_1}^2. \quad (\text{A.10})$$

We note that the whiteners of residual ICI can be any scaled version of square root of \mathbf{K}_z^{-1} given above. Consequently, the normalized autocorrelation matrix of residual ICI is a good choice instead of \mathbf{K}_z . After normalizing \mathbf{K}_z with $\sigma_{c_k}^2$, the whiteners of residual ICI approximates to a constant matrix.

Values of the Whiteners of Residual ICI Plus Noise

At finite SNR, consider the setting $\{K = 1, q = 1, p = 2\}$ as (A.1), for which the covariance matrices \mathbf{K}_z of residual ICI plus noise ($Z_m = c_{m,k} + W_m$) is given by

$$\mathbf{K}_z|_{\{K=1,q=1,p=2\}} = \begin{bmatrix} 1 & 0 & 0 \\ 0 & 1 & 0 \\ 0 & 0 & 1 \end{bmatrix} \sigma_W^2 + \begin{bmatrix} 1 & 0.775 & 0.645 \\ 0.775 & 1 & 0.775 \\ 0.645 & 0.775 & 1 \end{bmatrix} \sigma_{c_1}^2. \quad (\text{A.11})$$

where $\sigma_W^2 = E[|W_m|^2]$ and $Z_m = c_{m,k} + W_m$.

After normalizing \mathbf{K}_z given in (A.11), the whitener of residual ICI plus noise approximates to a matrix only depends on $\sigma_{c_1}^2/\sigma_W^2$. It is straightforward to extend this property to the other settings of $\{q, p, K\}$.

Gains of the Whiteners of Residual ICI

We consider the four cases

1. $\{K = 0, q = 1, p = 1\}$,
2. $\{K = 1, q = 1, p = 2\}$,
3. $\{K = 1, q = 1, p = 1\}$,
4. $\{K = 2, q = 1, p = 1\}$, all at infinite SNR.

The corresponding \mathbf{K}_z matrices are given above.

By (4.11), the resulting post- to pre-whitening SINR ratios are 2.0588, 2.9258, 8.7052, and 35.25, respectively.

Please note that the pre-whitening SINR of case (3) and (4) are worse than case (2). If we compare the post-whitening SINR of case (2), (3) and (4) with the conventional SINR E_s/σ_{c1} , the resulting SINR ratios of case (2), (3) and (4) will be 2.9258, 5.7146, and 24.94 times better than E_s/σ_{c1} , respectively. In Fig. 4.6, the difference of SINR between unwhitening and $\{K = 1, q = 1, p = 1\}$ methods is close to 5.7146 (7.57 dB). Simulation confirms theory.

However, the mathematical relation between SINR and bit error rate (BER) is not straightforward. The proposed MLSE of $\{K = 2, q = 1, p = 1\}$ indeed provides a lower error floor than $\{K = 1, q = 1, p = 1\}$ with perfect CSI assumed. But Fig. 5.1 shows that the two proposed MLSE have very close and indistinguishable performances at practical SNR. As a result, we provide $\{K = 1, q = 1, p = 1\}$ as the default setting of the proposed MLSE detection. Furthermore, we provide $\{K = 2, q = 1, p = 1\}$ as the default setting of the proposed MMSE/iterative MMSE for its significant SNR improvement.

Simulation of the Imperfect Whiteners

As mentioned, the whitener of residual ICI plus noise approximates to a matrix only depends on σ_{c1}^2/σ_W^2 . For $\{K = 1, q = 1, p = 1\}$, we have the whitener as

$$\begin{bmatrix} \frac{\sigma_{W/c1}^2+1.785}{\sigma_{W/c1}^2+1} & 1.16\frac{1}{\sigma_{W/c1}^2+1} & 1.16\frac{1}{\sigma_{W/c1}^2+1} \\ 1.16\frac{1}{\sigma_{W/c1}^2+1} & 1 & 1.16\frac{1}{\sigma_{W/c1}^2+1} \\ 1.16\frac{1}{\sigma_{W/c1}^2+1} & 1.16\frac{1}{\sigma_{W/c1}^2+1} & \frac{\sigma_{W/c1}^2+1.785}{\sigma_{W/c1}^2+1} \end{bmatrix} \quad (\text{A.12})$$

and for $\{K = 2, q = 1, p = 1\}$

$$\begin{bmatrix} \frac{\sigma_{W/c1}^2+1.62}{\sigma_{W/c1}^2+1} & 1.17\frac{1}{\sigma_{W/c1}^2+1} & 1.17\frac{1}{\sigma_{W/c1}^2+1} \\ 1.17\frac{1}{\sigma_{W/c1}^2+1} & 1 & 1.17\frac{1}{\sigma_{W/c1}^2+1} \\ 1.17\frac{1}{\sigma_{W/c1}^2+1} & 1.17\frac{1}{\sigma_{W/c1}^2+1} & \frac{\sigma_{W/c1}^2+1.62}{\sigma_{W/c1}^2+1} \end{bmatrix} \quad (\text{A.13})$$

where $\sigma_{W/c1}^2$ denotes σ_W^2/σ_{c1}^2 .

It seems reasonable to assume that $\sigma_{W/c1}^2$ will be estimated first and apply to (A.12) and (A.13) when we estimate the whitener's coefficients. We also assume a mismatch model of NIR: $\widetilde{\sigma_{W/c1}^2} = \gamma \times \sigma_{W/c1}^2$, where γ is a factor related to estimation error. When $\gamma = 1$, it means a perfect estimation $\sigma_{W/c1}^2$ without error. Figs. A.1 shows some simulation results for the TU6 channel. These results show that the mismatched NIR $\widetilde{\sigma_{W/c1}^2}$ can be 0.25 times or 2 times as $\sigma_{W/c1}^2$ without performance loss in proposed MLSE $\{p = q = K = 1\}$. Similarly, in proposed MMSE $\{p = q = K = 2\}$, the tolerance of mismatched NIR ranges from 0.7 to 1.05 times as $\sigma_{W/c1}^2$.

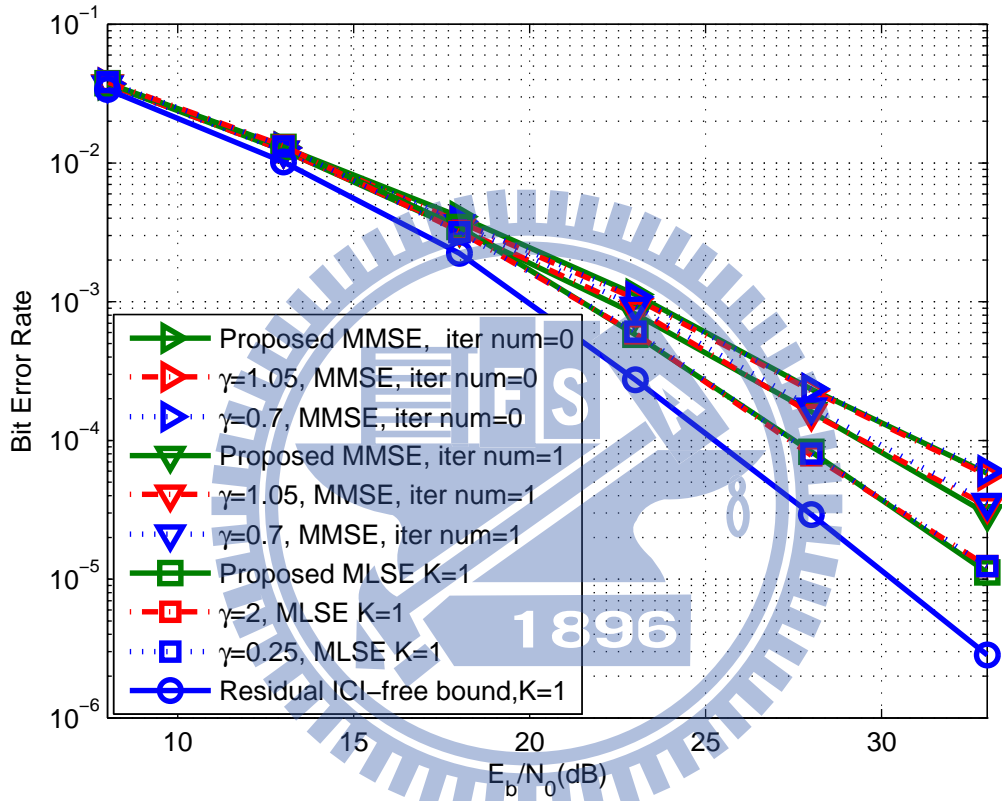
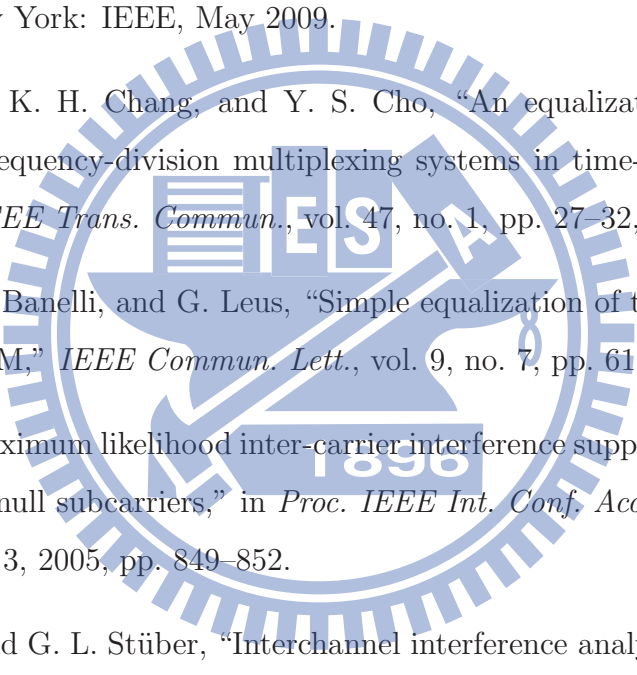


Figure A.1: Performance of proposed MLSE $p = q = K = 1$ and MMSE $p = q = 1, K = 2$, with imperfect whitener in the TU6 channel, at $N = 128$ and $T_{sa} = 714$ ns $f_d T_{sa} N = 0.137$ and under QPSK subcarrier modulation.

Bibliography

- 
- [1] IEEE Std. 802.16-2009, *IEEE Standard for Local and Metropolitan Networks — Part 16: Air Interface for Fixed and Mobile Broadband Wireless Access Systems*. New York: IEEE, May 2009.
- [2] W. G. Jeon, K. H. Chang, and Y. S. Cho, “An equalization technique for orthogonal frequency-division multiplexing systems in time-variant multipath channels,” *IEEE Trans. Commun.*, vol. 47, no. 1, pp. 27–32, Jan. 1999.
- [3] L. Rugini, P. Banelli, and G. Leus, “Simple equalization of time-varying channels for OFDM,” *IEEE Commun. Lett.*, vol. 9, no. 7, pp. 619–621, July 2005.
- [4] S. Ohno, “Maximum likelihood inter-carrier interference suppression for wireless OFDM with null subcarriers,” in *Proc. IEEE Int. Conf. Acoust. Speech Signal Process.*, vol. 3, 2005, pp. 849–852.
- [5] M. Russell and G. L. Stüber, “Interchannel interference analysis of OFDM in a mobile environment,” in *IEEE Veh. Technol. Conf.*, vol. 2, July 1995, pp. 820–824.
- [6] A. A. Hutter, J. S. Hammerschmidt, E. de Carvalho, and J. M. Cioffi, “Receive diversity for mobile OFDM systems,” in *Proc. IEEE Wirel. Commun. Networking Conf.*, Sep. 2000, pp. 707–712.
- [7] S. Ohno and K. A. D. Teo, “Approximate BER expression of ML equalizer for OFDM over doubly selective channels,” in *Proc. IEEE Int. Conf. Acoust. Speech Signal Process.*, 2008, pp. 3049–3052.

- [8] Y.-H. Yeh and S.-G. Chen, "An efficient fast-fading channel estimation and equalization method with self ICI cancellation," in *Eur. Signal Process. Conf.*, Sep. 2004, pp. 449–452.
- [9] H.-w. Wang, D. W. Lin, and T.-H. Sang, "OFDM signal detection in doubly selective channels with whitening of residual intercarrier interference and noise," in *IEEE Veh. Technol. Conf.*, May 2010, pp. 1–5.
- [10] W. C. Jakes, *Microwave Mobile Communications*. New York: Wiley, 1974.
- [11] Y. Li and L. J. Cimini, Jr., "Bounds on the interchannel interference of OFDM in time-varying impairments," *IEEE Trans. Commun.*, vol. 49, no. 3, pp. 401–404, Mar. 2001.
- [12] G. Huang, A. Nix, and S. Armour, "DFT-based channel estimation and noise variance estimation techniques for single-carrier FDMA," in *IEEE Veh. Technol. Conf. Fall*, Sep. 2010, pp. 1–5.
- [13] G. L. Stüber, *Principles of Mobile Communication*, 2nd ed. Boston, MA: Kluwer Academic, 2001.
- [14] Y.-S. Choi, P. J. Voltz, and F. A. Cassara, "On channel estimation and detection for multicarrier signals in fast and selective rayleigh fading channels," *IEEE Trans. Commun.*, vol. 49, pp. 1375–1387, Aug. 2001.
- [15] X. Cai and G. B. Giannakis, "Bounding performance and suppressing intercarrier interference in wireless mobile OFDM," *IEEE Trans. Commun.*, vol. 51, no. 12, pp. 2047–2056, Dec. 2003.
- [16] C.-Y. Hsu and W.-R. Wu, "Low-complexity ICI mitigation methods for high-mobility SISO/MIMO-OFDM systems," *IEEE Trans. Veh. Technol.*, vol. 58, no. 6, pp. 2755–2768, July 2009.
- [17] D. Huang, K. B. Letaief, and J. Lu, "Bit-interleaved time-frequency coded modulation for OFDM systems over time-varying channels," *IEEE Trans. Commun.*, vol. 53, no. 7, pp. 1191–1199, July 2005.

- [18] H.-D. Lin, T.-H. Sang, and D. W. Lin, "BICM-OFDM for cooperative communications with multiple synchronization errors," in *Proc. Int. Wirel. Commun. Mobile Comput. Conf.*, July 2010, pp. 1055–1059.
- [19] K.-C. Hung and D. W. Lin, "Pilot-aided multicarrier channel estimation via MMSE linear phase-shifted polynomial interpolation," *IEEE Trans. Wirel. Commun.*, vol. 9, no. 8, pp. 2539–2549, Aug. 2010.
- [20] H. Stark and J. W. Woods, *Probability and Random Processes with Applications to Signal Processing*, 3rd ed. Upper Saddle River, New Jersey: Prentice-Hall, 2002.
- [21] A. F. Molisch, *Wireless Communications, 2nd ed.* Chichester, West Sussex, UK: Wiley, 2011.
- [22] P. Schniter, "Low-complexity equalization of OFDM in doubly selective channels," *IEEE Trans. Signal Process.*, vol. 52, no. 4, pp. 1002–1011, Apr. 2004.
- [23] S. U. Hwang, J. H. Lee, and J. Seo, "Low complexity iterative ICI cancellation and equalization for OFDM systems over doubly selective channels," *IEEE Trans. Broadcasting*, vol. 55, no. 1, pp. 132–139, Mar. 2009.
- [24] A. A. Hutter and R. Hasholzner, "Determination of intercarrier interference covariance matrices and their application to advanced equalization for mobile OFDM," in *Proc. 5th Int. OFDM Workshop*, Hamburg, Germany, Sep. 2000, pp. 33-1–33-5.
- [25] H.-w. Wang, D. W. Lin, and T.-H. Sang, "OFDM signal detection in doubly selective channels with whitening of residual intercarrier interference and noise," *IEEE J. Sel. Areas Commun.*, vol. 30, no. 4, pp. 684-694, May 2012.
- [26] H. V. Poor, *An Introduction to Signal Detection and Estimation, 2nd ed.* New York: Springer, 1994.
- [27] H. Lee and I. Lee, "New approach for coded layered space-time OFDM systems," in *IEEE Int. Conf. Commun.*, vol. 1, May 2005, pp. 608–612.

- [28] H. Lee, B. Lee, and I. Lee, "Iterative detection and decoding with an improved V-BLAST for MIMO-OFDM systems," *IEEE J. Sel. Areas Commun.*, vol. 24, no. 3, pp. 504–513, Mar. 2006.
- [29] L. Papke, and P. Robertson, "Improved decoding with SOVA in a parallel concatenated (turbo-code) scheme," in *IEEE Int. Conf. Commun.*, 1996, pp. 102–106.
- [30] J. Vogt and A. Finger, "Improving the MAX-LOG-MAP turbo decoder," *Electron. Lett.*, vol. 36, pp. 1937–1939, Nov. 2000.
- [31] M. C. Jeruchim, P. Balaban, and K. S. Shanmugan, *Simulation of Communication Systems - Modeling, Methodology, and Techniques*, 2nd ed. Kluwer Academic/Plenum Publishers, 2000.
- [32] P. A. Bello, "Characterization of randomly time-variant linear channels," *IEEE Trans. Commun. Syst.*, vol. CS-11, no. 4, pp. 360V393, Dec. 1963.
- [33] G. L. Turin et al., "A statistical model of urban multipath propagation," in *IEEE Veh. Technol. Conf.*, vol. VT-21, Feb. 1972, pp. 1–9.
- [34] J. G. Proakis, *Digital Communications*, 4th ed. McGraw-Hill, 2001.
- [35] R. H. Clarke, "A statistical theory of mobile-radio reception," *Bell Sys. Tech. J.*, vol. 47, no. 6, pp. 957V1000, July-Aug. 1968.
- [36] A. Papoulis, *Probability, Random Variables, and Stochastic Processes*, 1st ed. McGraw-Hill, 1965.
- [37] M. J. Gans, "A power-spectral theory of propagation in the mobile-radio environment," in *IEEE Veh. Technol. Conf.*, vol. VT-21, Feb. 1972, pp. 27–38.
- [38] A. Papoulis, *Mobile Fading Channels*, Wiley, 2002.
- [39] C.-D. Iskander, "A MATLAB-based object-oriented approach to multipath fading channel simulation," *White Paper, MathWorks, Natick, MA*, [Online]. Available: <http://www.mathworks.com/matlabcentral/?leexchange/18869>.

- [40] H.-w. Wang, D. W. Lin, and T.-H. Sang, "LMMSE detection of OFDM signals in time-varying channels with partial whitening of intercarrier interference and soft decision feedback, *IEEE WPMC. Conf.*, 2012, accepted.



簡 歷

Hai-wei Wang received the B.S. degree in control engineering and the M.S. degree in electronics engineering from National Chiao Tung University, Hsinchu, Taiwan, R.O.C., in 1995 and 1999, respectively. She was with Silicon Integrated Systems Corp., Hsinchu, during 1999–2002 and with Realtek Semiconductor Corp., Hsinchu, during 2002–2004. She is currently pursuing the Ph.D. degree in electronics engineering from the National Chiao Tung University. Her research interests are in the areas of digital communications and communication theory.



著作目錄

- Journal articles

- H.-w. Wang, D. W. Lin, and T.-H. Sang, OFDM signal detection in doubly selective channels with whitening of residual intercarrier interference and noise, *IEEE J. Sel. Areas Commun.*, vol. 30, no. 4, pp. 684-694, May 2012.

- Conference and proceeding papers:

- H.-w. Wang, D. W. Lin, and T.-H. Sang, OFDM signal detection in doubly selective channels with whitening of residual intercarrier interference and noise, in *IEEE Veh. Technol. Conf.*, May 2010, pp. 1V5.
- H.-w. Wang, D. W. Lin, and T.-H. Sang, LMMSE detection of OFDM signals in time-varying channels with partial whitening of intercarrier interference and soft decision feedback in *IEEE WPMC. Conf.*, 2012, accepted.
- H.-w. Wang, D. W. Lin, K.-C. Hung, and Y.-T. Lee, "Design and DSP software implementation of mobile WIMAX baseband transceiver functions," in proceedings of the 2007 conference on Emerging direction in embedded and ubiquitous computing, ser. *EUC'07*. Berlin, Heidelberg: Springer-Verlag, 2007, pp. 181-192.